Article:
Qiu, W., Pham, T.K., Zou, X. et al. (2 more authors) (2017) Natural mutagenesis-enabled global proteomic study of metabolic and carbon source implications in mutant thermoacidophillic Archaeon Sulfolobus solfataricus PBL2025. Journal of Proteome Research. ISSN 1535-3893

https://doi.org/10.1021/acs.jproteome.6b00920

Journal of proteome research

Article

Natural mutagenesis-enabled global proteomic study of metabolic and carbon source implications in mutant thermoacidophillic Archaeon *Sulfolobus solfataricus* PBL2025

Wen Qiu, Trong Khoa Pham, Xin Zou, Saw Yen Ow, and Phillip C. Wright

J. Proteome Res., **Just Accepted Manuscript** • Publication Date (Web): 17 May 2017

ACS Publications

Journal of Proteome Research is published by the American Chemical Society. 1155 Sixteenth Street N.W., Washington, DC 20036

Natural mutagenesis-enabled global proteomic study of metabolic and carbon source implications in mutant thermoacidophillic Archaeon *Sulfolobus solfataricus* PBL2025.

Wen Qiu[1,2], Trong Khoa Pham[1], Xin Zou[3], Saw Yen Ow[4] and Phillip C. Wright[1,5]*

[1] ChELSI Institute, Department of Chemical and Biological Engineering, the University of Sheffield, Mappin Street, Sheffield, S1 3JD, United Kingdom

[2] State Key Laboratory of Rice Biology, Institute of Biotechnology, Zhejiang University, Hangzhou, 310058, China

[3] Ministry of Education Key Laboratory of Systems Biomedicine, Shanghai Centre for Systems Biomedicine, Shanghai Jiao Tong University, Shanghai, 200240, China

[4] CSL Limited, 45 Poplar Road, Parkville, Victoria 3052, Australia

[5] Now at: School of Chemical and Advanced Materials, Faculty of Science, Agriculture and Engineering, Newcastle University, Newcastle upon Tyne, NE1 7RU, United Kingdom

*Corresponding author: Phillip C. Wright

Tel: +44 (0)191 208 5556

E-Mail: phillip.wright@newcastle.ac.uk

HIGHLIGHTS

- Systems-level study of mutagenesis directed shifts, as well as carbon source dependency in Archaeal subsystems using the model organism, *Sulfolobus solfataricus* P2 and bioengineering model PBL2025 using quantitative proteomics and metabolomics.
- Over 20% of the observed proteome showed differential regulation, with major inductions along energy and carbohydrate metabolism, as well as novel compensation mechanisms in *S. solfataricus* strains when grown on different carbon sources.
- Our findings indicate differences in the feedback mechanisms through the activation of carbon fixation pathways (in PBL2025), and down-regulation of nucleotide metabolism (in P2), followed by collective, but distinct, re-balancing of amino acid

anabolism/metabolism processes employed by the spontaneous mutant strains to adapt to changes of carbon sources.

ABSTRACT

The thermoacidophilic crenarchaeon *Sulfolobus solfataricus* has been widely used as a model organism for archaeal systems biology research. Investigation using its spontaneous mutant PBL2025 provides an effective metabolic baseline to study subsequent mutagenesis-induced functional process shifts as well as changes in feedback inhibitions. Here, an untargeted metabolic investigation using quantitative proteomics and metabolomics was performed to correlate changes in *S. solfataricus* strains P2 against PBL2025 and under both glucose and tryptone. The study is combined with pathway enrichment analysis to identify prominent proteins with differential stoichiometry. Proteome level quantification reveals that over 20% of the observed overlapping proteome is differentially expressed under these conditions. Metabolic-induced differential expressions are observed along the central carbon metabolism, along with 12 other significantly regulated pathways. Current findings suggest that PBL2025 is able to compensate through the induction of carbon metabolism, as well as other anabolic pathways such as Val, Leu and iso-Leu biosynthesis. Studying protein abundance changes after changes in carbon sources also reveals distinct differences in metabolic strategies employed by both strains, whereby a clear down-regulation of carbohydrate and nucleotide metabolism is observed for P2, while a mixed response through down-regulation of energy formation and up-regulation of glycolysis is observed for PBL2025. This study contributes, to date, the most comprehensive network of changes in carbohydrate and amino acid pathways using the complementary systems biology observations at the protein and metabolite levels. Current findings provide a unique insight into molecular processing changes through natural (spontaneous) metabolic rewiring, as well as a systems biology understanding of the metabolic elasticity of thermoacidophiles to environmental carbon source change; potentially guiding more efficient directed mutagenesis in archaea.

KEYWORDS: *Sulfolobus solfataricus,* carbon source, iTRAQ, enrichment analysis, proteomics, metabolomics, quantitative metabolic pathways.

BIOLOGICALSIGNIFICANCE

Our data describes the comprehensive proteome and metabolome maps for the survival of *S. solfataricus* due to a large number of missing genes, as well as their systematic adaptation to carbon source stimuli from glucose to tryptone respectively.

One important finding of this investigation is the identification of corresponding proteins belonging to various ABC transporters functioning for *S. solfataricus* P2 or PBL2025 strains and the indication of different substrate (carbohydrate/peptide) binding activity, which provides clues for efficient characterisation of the substrate transport system.

Our study demonstrates increased protein expressions involving post translational modifications (PTMs) for carbon source stimuli from glucose to tryptone in P2 and candidate proteins were listed for future PTM modulation study involving, for instance, the phosphoproteome.

Our global proteomics and metabolomics datasets together support the hypothesis that the regulation of carbon source change from glucose to tryptone in *S. solfataricus* may involve a feedback-inhibition mechanism.

INTRODUCTION

The thermoacidophilic crenarchaeon *Sulfolobus solfataricus* is an industrially relevant model organism, with the ability to survive and grow in high temperature of 80°C and low pH of 3 (1). Further, it is able to utilise a variety of sugars and amino acids as the sole carbon and energy sources (2). *S. solfataricus* P2 was first isolated in Italy (3), whilst *S. solfataricus* PBL2025 strain (a spontaneous mutant of *S. solfataricus* 98/2 strain(s)) was isolated in the USA (4). With a fully sequenced genome of about a 3 Mbp consisting of a single chromosome and encoding 2977 proteins (5), *S. solfataricus* P2 has been widely used as a model microorganism to study crenarchael metabolism, while *S. solfataricus* PBL2025 represents a well-known biological host for further direct or indirect mutagenesis analysis (6). Comparatively, the spontaneous mutant PBL2025 lacks a series of genes from *SSO3004* to *SSO3050* (7), of which 6 genes are supposedly critical for central carbohydrate metabolism

(CCM), 8 genes in energy metabolism, 6 separate transporters, and 2 genes related to the formation of biofilms and secretion of extracellular polymeric substances (EPS) (8).

Glucose or tryptone used as a sole source of carbon and energy for *S. solfataricus* induces different metabolic enzymes, transporters and uptake systems to support growth and cell survival. In 2006, using ^{15}N metabolic labelling based proteomics, Snijders *et al.,*(9) reported that over 3% of the identified genes and 14% of the identified proteins in wild type P2 were differentially regulated, and were primarily involved in CCM. Recently, Esser *et al.* (10) have also speculated that sugar degradation pathways were blocked and gluconeogenesis enzymes of *S. solfataricus* were activated when tryptone was supplied. Further data supported by Esser *et al*., (10) also found that the phosphoproteome of the P2 strain was significantly affected during the onset of carbon source changes from basic sugars to tryptone.

In contrast to the extensively studied P2 strain, a comprehensive proteomics study has not been reported for strain PBL2025, an important metabolic engineering model. Interest and justification to study both *S. solfataricus* strains P2 and PBL2025 as a collective analysis is also driven by the discovery of their varying attachment affinity to various surfaces and the observation of different biofilm formation (11). Further interest also lies in identifying any unique enzymes involved in formation of extracellular polysaccharides in P2, which are supposedly absent in the spontaneous mutant (8).

Thus, to improve the understanding of metabolic processes between P2 and PBL2025 grown under identical stimuli and carbon sources, further investigation at the metabolic level is required. To achieve this, we applied an isobaric mass protein labelling technique coupled with tandem mass spectrometry. Further analysis using pathway-directed bioinformatics is also applied to identify prominent pathways affected by changing the carbon sources.

In addition to observations at the protein level, metabolite level monitoring was also performed using GC-MS analysis. In this study, we attempt to combine our observations at the quantitative proteome level with observations at the metabolome level to reveal potentially collective and unique response of the different *S. solfataricus* strains grown on different model carbon sources.

MATERIALS AND METHODS

Growth conditions

S. solfataricus strains P2 and PBL2025 were grown in media containing either 0.2% tryptone (w/v) or 0.4% glucose (w/v) as sole carbon and energy sources in a horizontal shaking thermal incubator (Thermotron, Infors, UK) at 120 rpm at 80°C. Cells grown on glucose was used as a control. Stock cultures of these strains were stored at -80°C and activated using either 0.4% glucose to grow up to OD_{650} = 1.0 ± 0.05, or 0.2% tryptone to grow up to OD_{650} = 0.70 ± 0.05. All experiments were performed at an initial OD_{650} of 0.2 ± 0.05 in 150 ml of standard media as described elsewhere (12). Cell growth curves were obtained by measuring the optical density at a wavelength of 650 nm using a spectrophometer (Ultrospec-2100 Pro UV/Visible, Amersham Biosciences, US) against time. The specific growth rates (μ) were calculated (biological triplicates) graphically by plotting OD_{650} *versus* time. The OD_{650} values were also corrected against evaporation (negative control without *S. solfataricus*).

Based on the growth curves, cells were collected at the late exponential growth phases for further experiments. A volume of 50 ml of cell culture was harvested and centrifuged at 5,000 x *g* for 10 min at 4°C and the cell pellet was collected and then stored at -80°C until required. Numbers of cells were counted using a haemocytometer (Marienfield, Germany) under an optical microscope (Axiostar Plus, USA). All chemicals were purchased from Sigma-Aldrich (Gillingham, UK) unless otherwise stated.

Quantitative proteomic studies

Protein extraction and iTRAQ labelling

Two sets of 8-plex iTRAQ experiments were performed to investigate the quantitative proteomes of these two strains when tryptone or glucose was used as a sole carbon source. Crude protein extraction was performed as described elsewhere (12). Briefly, cells were washed with extraction buffer (500 mM TEAB, triethylammonium bicarbonate pH8.5 containing 0.05% SDS (w/v)). Then re-suspended in the extraction buffer and one volume of acid washed glass beads (425-600 μm) (compared to cell pellet) was added. Protein was extracted using a disruptor (Genie Vortex, USA). Supernatants containing soluble crude extracts were centrifuged at 21000 × *g* for 30 min at 4 ℃ and then transferred into low binding tubes. To purify proteins, 5 times volumes of ice-cold acetone (compared to sample)

were added and samples were left at -20 ℃ overnight. Samples were centrifuged at 21000 × *g* for 20 min at 4 ℃; these protein pellets were then re-suspended in the extraction buffer, and protein concentrations were determined using the Bio-Rad RC-DC Protein Quantitation Assay (Bio-Rad, UK).

A total of 100 µg proteins of each phonotype was firstly reduced with 50 mM tris 2-carboxyethyl phosphine hydrochloride at 60 ℃ for 1h, then alkylated with 200 mM methyl methanethiosulfonate at room temperature for 10 min before being digested by trypsin at a ratio of 1:40 (trypsin:protein) at 37 ℃ overnight. Digested samples were then labelled using 8-plex iTRAQ reagents according to the manufacturer's protocol (ABSciex, USA). After labelling, samples were mixed and dried in a vacuum concentrator (Eppendorf Concentrator 5301, Germany). The detailed labelling of samples is shown in Tables 1A and B.

Hydrophilic Interaction Chromatography (HILIC)

Labelled peptides were re-suspended in 90 µl of HILIC buffer A (80% ACN, 10 mM ammonium formate, pH 3) prior to loading onto a 4.6 x 200 mm Poly HYDROXYETHYL-A column (5µm, 200Å, Hichrom Limited, UK) coupled with an Agilent 1100 Series HPLC system (Agilent, US) consisting of a G1311 Quat Pump, G1379 Degasser and G1314A UWD UV detector operated at a wavelength of 280 nm. Peptides were fractionated using a gradient as follows: 10 min of buffer A before ramping up to 20% of buffer B (5% ACN, 10mM ammonium formate, pH 5) for 5 min then up to 60% of buffer B for 50 min, then ramped up to 100% of buffer B for 10 min and kept for 10 min and finally 0% of buffer B for 5 min at a flow rate of 0.5 ml/min. Fractions were collected every minute, then 35 high intensity fractions were chosen and dried in a vacuum concentrator.

LC-MS/MS and Data Analyses

Each dried HILIC fraction was re-dissolved in 20 µl of MS loading buffer containing 3% acetonitrile and 0.1% formic acid, and then 10µl of sample was introduced to a nano-LC-ESI-qQ-TOF-MS/MS, QStarXL Hybrid ESI Quadrupole time of flight-tandem mass spectrometer, (Applied Biosystems, Framingham, MA; MDS-Sciex, Concord, Ontario, Canada). Details of the nano-LC system, MS/MS parameters and LC gradient used are described in details elsewhere (12).

Protein identification and quantitation were mainly carried out as described elsewhere (13). Briefly, MS/MS raw data were firstly converted into MGF format using a Mascot dll script in Analyst QS v. 1.1. Data were then submitted to a Phenyx search engine (v.2.6, Geneva Bioinformatics, Switzerland) using the *S. solfataricus* P2 protein database (2994 proteins) downloaded in April 2014 from NCBI (http://www.ncbi.nlm.nih.gov). Parameters for searching were set up as follows: MS tolerance was set at 0.4 Da and MS/MS tolerance was set as following: peptide tolerance 0.2 Da, charge +2 and +3, +4, minimum peptide length, *z*-score, maximum *p*-value and AC score were 5, 5, 10^{-6} and 5, respectively, and trypsin enzyme was used with two missed cleavages permitted for both cases. Modifications were set: 8-plex iTRAQ mass shifts (+304 Da, K and N-term) and methylthiol (+46 Da) as fixed modification and oxidation of methionine (+16 Da) as variable modification. The results were then exported to Excel (Microsoft 2010, USA) for further analyses. These data were also searched using a reversed *S. solfataricus* P2 database to estimate the false-discovery rate (FDR), as detailed elsewhere (14). Data were then analysed using our in-house statistical approach to determine regulated proteins (13).

The quantified proteins were categorized based on the arCOG functional code (http://archaea.ucsc.edu/arcogs/). Furthermore, to gain an understanding of how different *S. solfataricus* strains responded to different carbon sources at the proteomic level and to determine which pathways were significantly regulated, an enrichment test analysis based on the hypergeometric distribution model was used as described in the equation below (15). A p-value was calculated for each pathway in every regulated group and pathways that achieved p-values < 0.05, were considered to be significantly affected.

$$y = f(k \mid N, M, n) = \frac{\binom{M}{k}\binom{N-M}{n-k}}{\binom{N}{n}}$$

Where: *N*: total number of predicted proteins. *M*: number of proteins that are annotated to an arCOG category for gene function enrichment analysis or a specific KEGG pathway enrichment analysis, respectively. *n*: number of up or down regulated proteins. *k*: number of proteins that are regulated and also annotated to specific KEGG pathways or gene functional categories.

Metabolomic studies

Metabolite extraction and sample preparation

For extraction of metabolites, cell pellets were washed by distilled water then centrifuged at 5,000 x g for 5min at 4°C. Subsequently, cells were re-suspended in 500 µl ice cold (-20°C) methanol containing an equivalent volume of acid washed glass beads (425−600µm) (compared to cell pellet volume). Global metabolites were extracted using a disruptor (Genie Vortex, USA) with 7 cycles alternately 45 sec of disruption and 2 min of incubation on ice between each run. Supernatants containing the soluble crude extracts were centrifuged at 13,000 × g for 30 min at 4°C, transferred and dried by a vacuum centrifugation. Global metabolites were derivatized as described in detail elsewhere (16). Briefly, dried samples were re-suspend in 25 µl of dimethylformamide contain 0.1% pyrimide and then 25 µl of N-methyltrifluoroacetmide was added. Samples were incubated at 80°C for 60 min before being used for GC-MS analysis. Nor-valine was used as an external standard and its derivatization followed the above procedure. Samples and external standard was mixed before GC-MS injection.

GC-MS analysis

GC-MS settings for global metabolome analyses were used as follows: analysis was performed on a GC coupled to a Finnigan Trace DSQ single Quadrupole GC-MS coupled to an auto-sampler (model AS3000, Thermo Electron, Waltham, USA) equipped with a 30 m × 0.25 mm × 0.25 µm df stabilwax fused silica column (Thames Restek, Bucks, UK). Hot needle injection with a 1 µl injection volume was employed. Helium was used as the carrier gas at a constant flow rate of 1 mL/min. The splitless injector was set to 250 ℃, running on the splitless mode. The oven temperature profiles were programmed to trace global metabolite: 40 ℃ held for 0.5 min, followed by a 30 ℃/min ramping up to 200 ℃ and held at 200 ℃ for 1 min.

The GC-MS was operated in full scan mode with a mass range covering from 50 to 650 m/z. The ionization temperature was applied at 230^{o}C and 10^{5} eV was also used for ionization process. A biological triplicate and a technical duplicate were performed for each sample.

Data processing and analysis

All chromatograms (raw data) were firstly converted into .mzXML format by MSConvert of ProteoWizard (version 3.0 4624). Identification of metabolites was achieved by searching against the NIST main library and extracted data was modified (to remove derivation information) using an in house Macros program (from Dr. Rahul Kapoore in the University of Sheffield). The mass spectrum (Xcalibur .raw file) was analysed using the Automated Mass Spectral Deconvolution and Identification System (AMDIS) (V2.70) to identify compounds by matching detected data with the mass spectral library, which linked to the National Institute of Standards and Technology (NIST) MS search 2.0 NIST 2011 (NIST 11, USA). A deconvolution issue needs to be considered which resulted from the shared fragment ions by co-eluting compounds. To achieve a better identification of even low abundance peaks in the TIC various and to determine the maximum number of components with the smallest false-positive hits, optimised parameters were used (17). The deconvolution settings for AMDIS were: scan direction: high to low; instrument type: quadrupole; adjacent peak subtraction, 0; resolution, high; sensitivity, high; shape requirements, medium with target compounds from main library; component width: 12 (signal to noise ratio will be better with small component width) with minimum match factor 60. After deconvolution, the match factor >60% and probability >20% were considered for which the experimental spectrum matches with NIST reference spectrum (18). The relative intensity ('area' extracted from AMDIS) was normalized against the area of Nor-valine, resulting in metabolite abundance was expressed as ratios relatives to external standard. Therefore, the abundance change between different samples can be compared in terms of 'relative change'.

Each metabolite was matched with a unique C number (entry number of metabolites in KEGG COMPOUND database), which was obtained by manually searching against the KEGG database (http://www.kegg.jp/kegg/kegg2.html). The related pathways were mapped by searching against the *S. solfataricus* database (19).

RESULTS AND DISCUSSIONS

Cell growth profiles

Strain PBL2025 compared to P2 grown on glucose

We observed similar growth profiles between PBL2025 and P2 grown on the standard glucose media (Figures 1A), though PBL2025 exhibited a significantly prolonged lag phase than P2 (18 hours compared to 10 hours). The growth differences might have been a result of the induced metabolic burden from the absence of genes *SSO3003-SSO3050* in PBL2505 (to be discussed in detail later). Briefly, as expected, six of these genes are composed of transporters, six others are believed to be involved in the CCM, while an additional 8 genes may assume roles in energy metabolism (7); their absence might potentially alter PBL2505 energy metabolism upon the onset of stationary phase.

As mentioned above, the longer onset of lag phase in PBL2025 might be a result of the absence of the ATP-binding cassette (ABC) transporters and secondary transporters compared to P2 (encoded by genes *SSO3012, SSO3043, SSO3045, SSO3046, SSO3047* and *SSO3048*), since the uptake of sugars is carried out *via* ABC and secondary transporters (20). However, compared to strain P2, the average specific growth rate of PBL2025 was higher on 0.4% glucose growth (Figure 1C), 0.0106 $\pm$ 0.002 and 0.0214 $\pm$ 0.0001 h^{-1} for P2 and PBL2025 respectively. Correspondingly, a slight increase of glucose consumption (35.6 mg L^{-1} h^{-1} compared to 40.2 mg $L^{-1}h^{-1}$, calculation based on Figure 1D) and a decrease of doubling time (32.5 $\pm$ 0.69 h compared to 65.4 $\pm$ 0.65 h) were also observed. Consequently, the higher growth rate could have been an effect of the activation of the existing ABC transporters, since the uptake of glucose is mediated by ABC-transporters in *S. solfataricus* (21), or *via* potential activation of other unknown/uncharacterised transport systems relative to P2, as proposed elsewhere (22). Earlier evidence from a study on cellodextrin consumption *via* directed mutagenesis in *S. solfataricus* 98/2 by Lalithambika (22) suggested that the inactivation of a putative ABC transporter involving Sso2847, Sso2848, Sso2849 and Sso2850 had no effect on the cell growth when grown on glucose. Accordingly, the authors proposed the existence of other additional transport systems in strain 98/2 relative to P2 (22). The information about ABC transporters gained in this study is to be discussed in the ‘‘Carbohydrate transporter proteins’’ section.

S. solfataricus strains grown on tryptone compared to glucose

The specific growth rates of *S. solfataricus* strains grown on 0.2% tryptone and 0.4% glucose are shown in Figure 1C. From Figure 1C, we can see the average specific growth rates of P2 were 0.0106 ± 0.002 h^{-1} and 0.0195 ± 0.001 h^{-1} when grown on glucose and tryptone respectively, whilst the specific growth rates of PBL2025 were 0.0214 ± 0.0002 h^{-1} and 0.0132 ± 0.002 h^{-1} respectively. The faster growth of P2 on tryptone compared to glucose was also reported in a previous study, where oligopeptide binding proteins (encoded by *SSO1273* and *SSO2619*) of ABC transporters were strongly induced by the addition of tryptone in the media (23). This also agrees with another study (20), where the glucose-binding proteins activity of ABC transporters in P2 was at the highest levels in tryptone compared to glucose, which was estimated by using radiolabeled sugars with and without presence of unlabeled sugar, since transport proteins are supposed to catalyse the transfer of carbon sources across membrane into the cell (24).

Both *S. solfataricus* P2 and PBL2025 strains had a shorter lag phase in tryptone than in glucose media: 4 h and 12h differences for tryptone compared to glucose for P2 and PBL2025 respectively. The shorter lag phase of these strains in tryptone conditions may result from the direct utilisation of it as tricarboxylic acid cycle (TCA) intermediates (25). This is because *S. solfataricus* can utilise various amino acids as carbon sources and synthesise all 20 amino acids (2) for protein biosynthesis and also as intermediate metabolites for carbohydrate, lipid and nucleotide metabolism due to the close interaction of amino acid metabolism with glycolysis, gluconeogenesis and the citrate cycle (26). By contrast, glucose metabolism in *S. solfataricus* is through the Entner-Doudoroff (ED) pathway: semi-phosphorylative and non-phosphorylative (np-ED) branch (27) before preceding to the TCA cycle, the intermediates of which are used as precursors for cellular biosynthesis. Furthermore, the replenishment of oxaloacetate in the ED pathway is necessary to keep the TCA cycling and it catalyze the initial reaction step of TCA cycling: oxaloacetate + Acetyl-CoA → citrate (25). In *S. solfataricus,* it occurs *via* carboxylation of pyruvate or phosphoenolpyruvate when grown on glucose (9), and the oxaloacetate can be gained directly from Asp/Ala in tryptone condition. All together this might explain why the growth of *S. solfataricus* strain P2 on tryptone was faster than in glucose. A further explanation is to be discussed in the section "Regulation of CCM for tryptone *vs* glucose conditions". Moreover,

the effect of media on cell biomass of the *S. solfataricus* strains was also estimated. Both strains had reduced biomass yields when grown on tryptone compared to glucose in the stationary phases (0.41 ± 0.04 compared to 0.81 ± 0.01 gL^{-1} for P2, and 0.43 ± 0.05 compared to 0.64 ± 0.06 gL^{-1} for PBL2025 respectively). This was a result of the limit of available carbon and energy sources in tryptone media compared to glucose.

In summary, *S. solfataricus* PBL2025 exhibited a longer lag phase than P2 when grown on glucose and a lower growth rate in tryptone media respectively, possibly due to the absence of several substrate uptake genes. In addition, both *S. solfataricus* P2 and PBL2025 strains could utilise tryptone as a sole carbon source, but demonstrated different growth rates on tryptone compared to glucose conditions: 1.25 fold faster for P2 and 1.62 fold slower for PBL2025 respectively. However, maximum cell biomasses for both *S. solfataricus* P2 and PBL2025 strains grown on tryptone were less than those grown on glucose.

The effect of pH changing during culturing of *S. solfataricus* on its growth behavior

To test if the lower OD observed for *S. solfataricus* strains growth on tryptone compared to glucose may be a consequence of the observed alkalisation of the growth medium, the pH of medium was measured against the growth at a wavelength of OD_{650nm} (Figure 2). We observed that the change of pH for glucose and tryptone media shows vastly different trends. Although both strains were grown on an initial pH of 3.04, our measured pH was observed to fall towards pH 2.3 on 0.4% glucose media, while pH rose towards pH 6.9 for the case when 0.2% tryptone was provided as a sole carbon source. We believe this can be attributed to the differing buffering capacities between the media, and corroborates with similar findings reported earlier (28). The drop of OD_{650} was observed for all the strains when the pH of the growth medium reached to the upper tolerance limit of cell membrane (pH 6.5-7.0) (29). It can be inferred that the low OD observed on 0.2% tryptone media may have contributed partly to the limit by up-taking of substrate, since cell growth was observed again when the tryptone medium was acidified to 3.04 and it stopped growing when the media pH reached ca. 6.5 (data not shown).

Proteomics results

Although numerous proteomics studies have been undertaken to study *S. solfataricus* P2, such comparable studies on strain PBL2025 are still limited. While there is a previous report

on carbon source dependence from tryptone to glucose against protein phosphorylation level in *S. solfataricus* P2 (10), the study focused heavily on phosphoproteome profiling and site mapping. Herein, we demonstrate an additional level of understanding through quantitation at these protein levels. To facilitate this investigation, two sets of 8-plex (8 labels) iTRAQ experiments were carried out to investigate the responses of these *S. solfataricus* strains (PBL2025 *vs* P2) against different carbon sources (tryptone *vs* glucose). Related details in experimental design are shown in Tables S1 and Figure S1 in the Supplementary materials.

A total of 740 proteins and 702 proteins were identified at FDR < 1% from the first and second iTRAQ experiments respectively. Further filtering of proteins resulting from two or more unique peptide sequences showed 609 and 583 proteins quantified respectively. These proteins were curated into a final list of identifications for further two-tailed t-test assessments at the 95% confidence interval to determine differentially regulated proteins (30). Additional fidelity was also provided from the obtained quantitative data through a gene functional analysis using protein functional categories and localization retrieved from arCOG (http://archaea.ucsc.edu/arcogs/) (31). This allowed the correlation of CCM to other significantly affected cellular processes *via* further pathway enrichment analysis (15). Details of these analyses are discussed below.

Characterisation, functional classification and localisation of regulated proteins

Amongst proteins quantified and considered as significantly regulated, cytoplasmic proteins were predominantly observed (approximately 50% for each phenotype comparison), followed generally by uncharacterised putative proteins (Supporting Information Table S2). Archaea generally possess a single cytoplasmic membrane and lack an outer periplasm, however, they contain proteins attached to the outer layer: the cytoplasmic membrane; commonly called pseudoperiplasm (32). Although frequently considered as low abundance proteins, we were successful at identifying a number of pseudoperiplasm proteins during our phenotype analysis. Using further pathway enrichment analysis (Table 3), other proteins associated with primary pathways such as amino acid biosynthesis and carbohydrate metabolism were also identified and found to be inhibited under tryptone compared to glucose conditions. Protein level profiles with evidence of inhibition were observed successfully for tryptone compared to glucose conditions on nucleotide metabolism in P2 and tryptone compared to glucose condition on energy metabolism in PBL2025, respectively. Other pathway annotations were also obtained from cellular genetic information processing infrastructures such as

transcription and translation. Further details are provided in Supporting Information Table S3. We observed that most of the regulated proteins observed in translational processsing were ribosomal proteins and tRNA synthetases, as well as proteins involved in amino acids biosynthesis (Figure 3 and Table S3).

Gene function enrichment analysis

Differentially regulated proteins were first assigned to different functional ontologies based on their gene functions (from arCOG) and subjected to gene functional analysis at a p-value < 0.05 (31). Regulated proteins were classified into 18 or 19 out of 26 arCOG functional categories in *S. solfataricus*. Key proportions from the different groups are depicted in Figures S2 A-C and S3 (detailed results in Supplementary Data Table S3). Gene function categories identified with less than 5 quantified proteins and those with only one regulated gene are not considered for classification.

From functional comparisons using *S. solfataricus* PBL2025 *vs* P2 grown on glucose, a lower relative abundance of energy production and conversion (arCOG C) and defence mechanism (arCOG V) categories were observed (Figure S2 A), while the higher abundance of lipid transport and metabolism (arCOG I) were identified.

Furthermore, enrichment analysis revealed that proteins of arCOG V (Defence mechanisms) and arCOG P (Inorganic ion transport and metabolism) were down regulated for tryptone *vs* glucose in both strains (Figures S2 B and C). Additional down regulated proteins were contributed into carbohydrate transport and metabolism (arCOG G) and transcription (arCOG K); while up regulated proteins belonging to arCOG O (posttranslational modification) were significantly observed in comparison of P2 grown on tryptone *vs* glucose (Figure S2 B). This agreed with observations reported elsewhere (10), in which a significant change of protein phosphorylation was found when provided with different carbon sources in P2 (10). The regulation of detoxification enzyme peroxiredoxin (Sso 2613) was detected here and the protein phosphorylation has been reported elewhere (10). Further study is required.

In summary, proteins belonging to defence mechanisms were regulated for all comparisons; regulation of proteins involved in transport systems were significantly affected in tryptone compared to glucose media for both strains.

Carbohydrate transporter proteins

The up/down-regulated transporters detected here are listed in Supporting Information Table S4. Furthermore, the affected transporters from previous studies where *S. solfataricus* was grown on other carbohydrates including ethanol, isopropanol, n-propanol, acetone, phenol with/without the presence of glucose (33-35) are also summarised in Table S4. We noticed that most of the quantified transporters in this investigation belonged to the ABC transporters (21).

In this study, we were able to quantify 10 ABC-transporter proteins, and 7 of them showed minimal differential abundance change, while an ATP-binding protein of ABC transporter (encoded by *SSO3055*) was observed with a higher abundance. A further sugar ABC transporter (encoded by *SSO 1168*) and an ATP-binding protein (encoded by *SSO2137*) were observed to be down-regulated in PBL2025 compared to P2 in glucose growth conditions.

Transporting of various substrates impacts on different parts of cellular metabolism and eventually growth patterns. Different transporters used to be discussed based on their substrate binding activities, which has been classified into carbohydrate and the di-/oligopeptide uptake super-families (36). Here, the up regulation of oligo/dipeptide superfamily transporters was observed in both strains (in tryptone compared to glucose). When P2 was grown on tryptone compared to glucose, 10 proteins belonging to 7 ABC transporters were quantified, but only one periplasmic dipeptide binding protein of dipeptide ABC transporter (encoded by *SSO2619*) was up regulated. However, 4 of 5 quantified ABC transporters including Sso1003, Sso1275, Sso2619 and Sso3055 were up-regulated when PBL2025 was grown on tryptone compared to glucose. Detailed discussion can be found in the ‘‘Regulation of *S. solfataricus* in tryptone *vs* glucose conditions’’ section.

Metabolomic results

Proteomics techniques have been widely performed with regarding to interpreting the unique metabolic pathways of *S. solfataricus* (37). By contrast, metabolomics studies are still very limited, except the study on the CCM response of P2 to optimal (80°C) and suboptimal (75°C) living temperatures under standard glucose media (12) and CCM changes in metabolites levels between 2-keto-3-deoxygluconate kinase deletion mutant strain PBL2025*Δ*3195 and PBL2025 grown on Brock media at 76°C (38). In addition, it is still

unclear on the correlation between protein expression level changes and metabolome changes in response to a change of carbon source. In this study, metabolite identification was achieved by searching against the NIST library and annotation of metabolites was achieved by using GC-MS raw data searched against AMDIS. The raw results were saved in .txt format. Further analyses were performed using Excel (Microsoft 2013, USA). These results were firstly simplified by Macros program to remove derivation. To gain high confidence identification, only compounds detected from all biological triplicates per phenotype were used (as shown in Table 2A); and, others were discarded. In total, 149 compounds were identified from all experiments and 81 of them were assigned a KEGG C number (results are listed in Table S5 in Supplementary materials). Only 15 of these metabolites have been reported previously (12). Some representative compounds are listed in Table 2B.

The numbers of compounds determined for different strains grown on either glucose or tryptone are listed and interpreted in a Venn diagram (Figures 3A-C). For instance, a high percentage of unique compounds was detected in PBL2025 compared to P2 strain (30/122 = 24.6% *vs* 8/100 = 8.0%, Figure 3A) when both were grown on glucose.

A similar number of identified metabolites were observed for P2 and PBL2025 strains: 139 and 131 respectively as shown in Figure 3C. Among these, a large number of compounds (88/139 = 63.3% *vs* 89/131=67.9) overlapped for tryptone *vs* glucose comparisons in both P2 and PBL2025 strains (Figures 3B-C).

Effect of different carbon sources on *S. Solfataricus* metabolic pathways

Proteins assigned into KEGG pathways

Regulated proteins were distributed into 54, 51 and 56 different pathways (a total of 78 pathways from KEGG: http://www.genome.jp/kegg/) for three comparisons (see Table 3 and S1 for details of comparisons), respectively. To gain a better understanding of how different *S. solfataricus* strains responded to different carbon sources, a relative frequency of the regulated enzymes in each pathway was calculated using the enrichment test (hypergeometric model) with a p-value < 0.05 (39) and the results are shown in Table 3. As listed in Table 3, the significantly affected pathways were involved in amino acids biosynthesis, carbohydrate metabolism, energy metabolism and nucleotide metabolism. A proteomic analysis showed

that the absence of genes *SSO3004-SSO3050* in PBL2025 likely resulted in different regulations of pathway metabolism. According to the pathway enrichment test (as detailed in Table 3), up-regulated proteins were involved in butanoate metabolism, Val, Leu and iso-Leu biosynthesis and carbon fixation pathway (40) for PBL2025 *vs* P2, both grown on glucose (comparison C1); and proteins involved in Ala, asp and glu metabolism and glycolysis metabolism show increased expression level for comparison C2 and C3, respectively.

Metabolites assigned into KEGG pathways

We detected 81 metabolites with assigned C numbers (listed in Supplementary Table S5) and 47 of them were involved in KEGG pathways that have not been reported in *S. solfataricus* (12) were also detected. Of 140 compounds detected from tryptone *vs* glucose for P2 strain, 24 compounds had reduced abundances, while most of them (116 compounds; 82.9%) had increased abundances. A total of 15 amino acids, 10 of them belonging to KEGG metabolic pathways, were detected by GC-MS (see Table 3B). Detailed to be discussed in ‘’Regulation of amino acid metabolism’’ section.

Regulation of central carbohydrate metabolism (CCM)

A total of 52, 52 and 51 proteins involving the CCM were quantified for comparisons C1, C2 and C3, respectively. According to the pathway enrichment test (as detailed in Table 3) proteins involved in butanoate metabolism were found to be up-regulated for C1, but no abundance changeS were detected for C2 and C3. Furthermore, a significant down and up regulation of proteins were observed in glycolysis metabolism for comparisons C2 and C3, respectively; while proteins involved in pyruvate metabolism were decreased in abundance in C2; and, no abundance change was detected in comparisons C1 and C3 (Figure 4A).

Regulation of CCM for PBL2025 vs P2

The increased abundance of some enzymes involved in the CMM pathway was expected. For instance, a higher abundance of glucose 1-dehydrogenase (gdh-1) was detected as indicated in Figure 4A. This can be related to the absence of gluconolactonase encoding gene *SSO3041* and gdh encoding gene *SSO3042*. Since previous studies show that the first few steps of the non-phosphorylative Entner-Doudoroff pathway (27) converts glucose to glucono-1,5-lactone then to gluconate, catalysed by glucose dehydrogenase (gdh-1, -2, and -3, encoded by *SSO3003*, *SSO3042* and *SSO3204* separately) and gluconolactonase (encoded by *SSO2705* and *SSO3041*) separately (9). It is obvious to assume the absence of Sso3041 and Sso3042 resulted in the accumulation and thus the requirement of a high expression level of gene

SSO3003. However, although the substrate specificity of gdh-3 (Sso3204) in P2 has been shown to specific to glucose (41), its expression level remained unaffected in PBL2025 (as shown in Figure 4A). The pentose phosphate pathway enzymes also had similar abundances, although PBL2025 lacks genes *SSO3032* and *SSO3036*.

Moreover, the formation and production amount of EPS in attachment to glass between PBL2025 and P2 have been showed previously, where extracellular materials were formed in the former (11). At the proteomic level, Sso3006 was quantified, but its abundance in PBL2025 was not different to that observed in P2 (both grown on glucose standard media). Current results thus indicate the modulation of EPS production by α-mannosidase (Sso3006) occurs neither at the quantitative proteome level nor at the transcript level as proposed elsewhere (8), where a role of *SSO3006* was confirmed by the complementarity of this gene in a recombinant strain of PBL2025, but no expression of *SSO3006* (by q-PCR) were reported upon surface attachment in P2 (11). In addition, the reduction of carbohydrate content in EPS of PBL2025 has been detected on the expression of β-galactosidase LacS (*SSO3019*) using photometric methods (8) and strong induced transcriptional expression (measured using q-PCR) of *SSO3019* has been reported upon surface attachment in P2 (11); however, regulation of Sso3019 was not detected here. The up-regulated proteins involved in propanoate metabolism included: Acetyl-CoA C-acetyltransferases (encoded by *SSO2061, SSO2062* and *SSO2625*), methylmalonate-semialdehyde dehydrogenase (Sso1218) and 4-aminobutyrate aminotransferase (Sso3211) for PBL2025 compared to P2 (both grown on glucose).

In addition to changes involving the CCM, the increased abundances of malate oxidoreductase (Sso3197) and 2-keto-3-deoxy gluconatealdolase (Sso2869) were found in PBL2025 compared to P2 (as shown in Figure 4A).

Regulation of CCM for tryptone vs glucose conditions

From Figure 4A, we can see that the down regulation of proteins in glycolysis and pyruvate metabolism was significant in P2 grown on tryptone compared to glucose (comparison C2). This observation supports a previous study reporting that sugar degradation was blocked in the presence of tryptone in P2 (10). However, proteins involved in glycolysis were increased in expression level and no abundance change was detected in pyruvate metabolism in the *S. solfataricus* PBL2025 strain grown on tryptone compared to glucose (comparison C3).

Moreover, up regulation of key proteins (Sso1907, Sso2044 and Sso3211) that linked amino acid and carbohydrate metabolism were observed in both C2 and C3 comparisons: detailed discussion can be found in the Section ‘‘Regulation of Ala, Asp and Glu metabolism". The specific reasons for those differences are not clear yet, but the absence of ABC transporter encoding genes in PBL2025, which are involved in tryptone uptake and *SSO3035, SSO3041* and *SSO3042* that functions in carbohydrate metabolism may provide some clues for the above observation. As mentioned before, 4 of the 5 quantified ABC transporters (Sso1003, Sso1275, Sso2619 and Sso3055) showed up regulation with the supplementation of tryptone compared to glucose for PBL2025. These observations supported the work carried out by Elferink *et al*., (20), who found the expression of glucose-binding activity of the membrane-bound sugar-binding proteins reached highest level in cells grown on tryptone. It was also consistent with a previous study (23), where a strong expression of Sso2619 and Sso1273 (oligopeptide binding protein) under the addition of tryptone conditions was reported. Interestingly, the expression of Sso0999 was not affected under tryptone conditions in both strains, which is consistent with previous work (23). Furthermore, no abundance change of Sso0999 under acetone conditions (34), whereby up-regulation under n-propanol (33) and ethanol (34, 35), and down-regulation in iso-propanol and phenol containing media has been observed. In summary, activation of different ABC transporters can be achieved through the induction of substrate binding activities under the supplement of various carbon sources. It is obvious to hypothesise that the up regulation of these proteins could lead to the fact that the activation of their present transporters, possibly, contributed to the up-regulation of the glycolysis/gluconeogenesis pathway, and consequently, resulted in a shorter lag phase and a faster growth on tryptone compared to glucose mediated growth of PBL2025. The growth of PBL2025 can be sustained through the up-regulation of ABC transporters and glycolysis pathway with the presence of tryptone. Taken together, this may explain the observation of a shorter lag phase of PBL2025 and P2 when both were grown on tryptone compared to glucose, despite the absence of some transporter encoding genes in PBL2025. However, the strain P2 grew faster than PLB2025 if both grew in the same carbon sources (either tryptone or glucose).

Furthermore, the tryptone supplementation for *S. solfataricus* P2 growth resulted in the detection of a higher abundance of TCA intermediates, for instance, à-Ketoglutaric acid. This observation agreed with a previous report indicating that the amino acids supplementation

from media led to an increase of TCA intermediates (25). But the TCA pathway remained unaffected for both C2 and C3 comparisons, as indicated when tryptone and yeast extract were supplied for *S. solfataricus* P2 (9). Up and down regulation of proteins involved in sp-ED and gluconeogenesis were also observed, but these proteins did not show significant differential regulation.

Detailed discussion on amino acid metabolism, for instance, the Glu metabolic pathway that links carbohydrate and amino acid metabolism, can be found in the following part. Altogether, these results provide evidence explaining why growth of these two *S. solfataricus* strains on tryptone was faster than on glucose, which is possibly due to the direct utilization of amino acids in tryptone condition.

Regulation of amino acid metabolism

In the proteome, most of the detected amino acid metabolic pathways were down-regulated except for metabolism of Ala, Asp and Glu, which was up-regulated when glucose was supplied compared to tryptone in strain P2 (Table 3). The presence of a feedback regulation mechanism is supported by the detection of high abundance of amino acids in tryptone growth medium. The differential abundances of these proteins and amino acids are shown in Table 3 and Figures 4A and B.

Catabolism of amino acids involves the removal of α-amino groups and then the carbon skeletons including pyruvate, Acetyl-CoA, Acetoacetyl-CoA and TCA cycle intermediates (oxaloacetate, fumarate, succinyl CoA and α-ketoglutarate). These metabolites are directly used for carbohydrate, nucleotide metabolism and other cellular processes (25). In this study, *S. solfataricus* cells ceased growth at *ca.* 40 h when tryptone was supplied for both strains, and their biomass yields were less than those obtained in the glucose condition (see Supplementary materials). This was possibly due to the lack of available carbon sources for cell construction. At the proteome level, the down regulation of amino acid biosynthesis pathways in the tryptone condition in both strains was unsurprising, since cells did not require the production of more amino acids to use as storage sources (42). Conversely, it also meant that the protein synthesis process occured based on its functional properties rather than a need to store extra amino acids, as mentioned elsewhere (42). A negative-feed-back regulation mechanism has been proposed for amino acid biosynthesis regulation, which

means that the end-product inhibits its own biosynthesis through affecting the biosynthetic enzyme activity (for a review see elsewhere (43)). In other words, the supplementation of external amino acids interferes with their intracellular formation. Subsequently, when microorganisms resort to an exogenous supplement of amino acids, their intracellular biosynthetic pathways tend to be blocked or shut down. This was observed, for instance, for Val (44) and iso-Leu biosynthesis in *E. coli* (45). A similar phenomenon has been found for anthranilate synthase in *S. solfataricus*, which catalyses the synthesis of anthranilate from chorismate and glutamine and is feedback-inhibited by tryptophan (46). In the light of this, we can reasonably speculate that the down regulation of the detected amino acids metabolic pathways followed a similar pattern.

Biosynthesis of some amino acids was significantly different between PBL2025 and P2 (Table 3 and Figure 4B) although *S. solfataricus* can synthesise all 20 amino acids (2). The up-regulation of proteins involved in these amino acid metabolism pathways indicates an accelerative utilisation of pyruvate. As shown in Figure 4B, the pyruvate production from malatate and KD(P)G catalysed separately by these enzymes seems to be preferentially utilised by the biosynthesis of Leu, Val and iso-Leu compared to other amino acids. Also, it can be pursued from the higher abundance of proteins involved in Leu, Val and iso-Leu metabolism, especially 3-isopropylmalate dehydratase subunits (encoded by *SSO2470* and *SSO2471*), dihydroxy-acid dehydratase (Sso3107), 3-isopropylmalate dehydrogenase (Sso0723) in PBL2015 compared to P2. Above all, more active amino acid pathways might contribute to the higher specific growth rate of PBL2025 compared to P2 when grown on glucose.

Regulation of Val, Leu and iso-Leu metabolism

Val, Leu and iso-Leu are hydrophobic branched-chain amino acids (BCAAs). We were able to identify significant down regulation of BCAAs metabolic pathways at the proteome level, and detect a high abundance of Leu for *S. solfataricus* grown on tryptone (Tables 2-3 and Figure 4B). In the current study, the down regulation of Val, Leu and iso-Leu metabolism might follow a feedback-inhibited pattern in *S. solfataricus* (46) as speculated above. From a biosynthetic aspect, the last four reactions are catalysed by the same four enzymes in the biosynthesis of Val, Leu and iso-Leu (Figure 4B), therefore, they are mostly discussed synchronically (43). Enzymes with multiple substrates such as 3-isopropylmalate dehydratase subunits (encoded by *SSO2470* and *SSO2471*) and ketol-acid reductoisomerase (encoded by

SSO0576) are easily affected by the existence of any of BCCAs substrates (Figure 4B). D-erythro-3-methylamate, 2-methylamate, (2S)-2-Isopropylmalate, 3-Isopropylmalate and (2R, 3S)-3-Isopropylmalate are substrates for Sso2470 and Sso2471 where (S)-2-Aceto-2-hydroxybutanoate, (R)-3-Hydroxy-3-methyl-2-oxopentanoate, (R)-2,3-Dihydroxy-3-methylpentanoate can be catalysed by Sso0576. Eventually, down regulation of BCCAs biosynthesis led to less conversion of succinyl-CoA or acetyl-CoA from these amino acids; and, then the inactivation of pyruvate metabolism and TCA cycle respectively (Table 3 and Figure 4B). Altogether, BCAAs metabolism indicates important biological roles in response to nutrient change from tryptone to glucose. The specific role of BCCAs in *S. solfataricus* need further investigation and the reported substantial studies of BCCAs in humans such as nutrient signaling, the regulation of protein synthesis in a variety of tissues, secondary structure of proteins as reviewed elsewhere (47) provide useful clues.

Regulation of Ala, Asp and Glu metabolism

For the tryptone *vs* glucose comparisons, most of the detected proteins were down regulated; only 0.5% and 0.8% of the quantified proteins were up regulated for P2 and PBL2025 respectively; these proteins were involved in Ala, Asp and Glu metabolism in P2, and Arg and Pro metabolism in PBL2025, as shown in Figure 4B. Increased levels of Glu and Pro were found for both strains grown under tryptone compared to glucose conditions (Figure 4B and Table 3B). Increased expression levels of NAD specific glutamate dehydrogenase (GDH; gdhA-1, gdhA-2 and gdhA-4, encoded by *SSO1457, SSO1907* and *SSO2044*, Figure 4B and Table S2 in the Appendix) were detected. These are responsable for Glu metabolism and catalyses the revisable oxidative deamination of Glu to produce 2-oxoglutarate and ammonia with reduction of NAD^+. Further, we observed an up regulation of 4-aminobutyrate aminotransferase (Sso3211, Figure 4B and Table S2), through which the extracellular Glu enters directly into the TCA cycle (Figure 4B). These observations agree with previous work, where certain concentrations of L-Glu and L-Asp enhanced cell growth by the presence of glucose, whereas Gly, L-Leu, L-Val showed no effect on cell growth (48). GDH is the key intermediate that links carbohydrate and amino acid (mainly from Glu, Pro, Arg and His) metabolism. GDH and Sso3122 play a key role in channeling the carbon skeletons of amino acids into the TCA cycle for gluconeogenesis during tryptone stimuli. This complementary information demonstrates concordance between findings from quantitative metabolomics and proteomic results.

Glu plays a central role in various metabolic processes, as well as stress responses in bacteria as reviewed elsewhere (49). Also, it has been reported that Glu-, Arg- and Lys-dependent acid resistance systems play an important role in protecting against acidic (50) and oxidative stress (51) in *E. coli*. Similar functions of Arg and Lys have also been found in *Salmonella typhimurium* CECT 443, but not for Glu (52). The growth-stimulation effect of L-Glu on the presence of glucose was significant compared to other amino acids (48) and a high abundance of Glu and Pro was detected in tryptone *vs* glucose comparisons for both strains (in Figure 4B). Glu catabolism is mainly carried out *via* the glutamate dehydrogenase (GDH) or glutamate decarboxylase (GAD) in bacteria (49). This aspect agrees well with the literature, which showed increased abundance of GDH in *S. solfataricus* (53).

Moreover, down regulation of glutamine synthetase (encoded by *SSO0366* and *SSO2440*) and high abundance of Gly detection was observed in this investigation for comparison C2. Glutamine synthetase is supposed to catalyse the synthesis of Gln from Glu and NH_3 (54). Its catalytic activity is solely regulated by end-product inhibition mechanism through Gly and Ala in *S. acidocaldarius* (55). The regulation of glutamine synthetase in *S. solfataricus* may indicate follow the end-product inhibition mechanism (Figure 4B).

In summary, the down regulation of most of the detected amino acid metabolic pathways may contribute greatly to the reduced life cycle of both strains (P2 and PBL2025) in tryptone compared to glucose.

Regulation of energy metabolism

Energy produced from various metabolic pathways is used for cell growth (25). For PBL2025 compared to P2 in glucose conditions, 5 of 21 quantified proteins involving the CO_2 fixation pathway were up-regulated. CO_2 fixation refers to the assimilation of CO_2 into cellular organic materials (56), which sustains autotrophic growth and can be also used for energy conservation and as a sink for cycling of reduced electron carriers, as discussed by Bar-Even, *et al.* (40). The mechanism for CO_2 assimilation in *Sulfolobus* is achieved by the 3-hydroxypropionate-4-hydroxybutyrate cycle (3HP/4HB) (57). Although not all of the enzymes have been characterized in the 3HP/4HB cycle, key genes in this pathway have been already found in *Sulfolobus* genomes, leading to the assimilation of bicarbonates (57).

Usually, this cycle is divided into two parts: (1) the transformation of acetyl-CoA and two bicarbonate molecules into succinyl-CoA, and (2) the conversion of succinyl-CoA into two acetyl-CoA molecules (57). Up-regulated proteins involving energy metabolism included acetyl-CoA C-acetyltransferase (acaB), acetyl-CoA synthetase (acsA) and aconitatehydratase. AcaB-2, acaB-3 and acaB-7 (encoded by *SSO2061, SSO2062* and *SSO2625* respectively) catalyse the conversion of acetoacetyl-CoA to acetyl-CoA, while protein acsA (encoded by *SSO2863*) catalyses the formation of acetyl-CoA from acetate. In addition, aconitatehydratase (encoded by *SSO1095*) catalyses the conversion of isocitrate to cis-aconitate, then to citrate. Acetyl-CoA is converted directly to pyruvate, propanoate metabolism as well as Val, Leu and Iso-Leu biosynthesis pathways (source: KEGG: http://www.genome.jp/kegg/). It can be inferred that the accumulation of acetyl-CoA involved in the regulation of intracellular biosynthesis metabolism, and further resulted in an activation of carbon fixation in PBL2025 and eventually a relatively higher growth rate of this strain than P2 (Figure 1A and 1C).

Under tryptone *vs* glucose conditions, no differentially-regulated proteins involved in energy-related pathways were found in P2. In contrast, 30 proteins involved in energy metabolism were found to be significantly regulated in PBL2025 (13 up and 17 down regulated). Statistically significant down regulation of oxidative phosphorylation proteins (based on pathway enrichment analysis) were observed in PBL2025 as a result of the unfriendly basic microenvironment conditions. Usually, NADH and succinate generated from the TCA cycle are oxidised and release energy to power the ATP synthase, subsequently ATP provides energy to other cellular process (58). In our investigation, inorganic pyrophosphatase (Sso2390) and three NADH dehydrogenases subunits C, D and I (Sso0323, Sso0324, and Sso0326) involved in the oxidative phosphorylation pathway were down regulated, but the ATP synthase (Sso0559, Sso0561, Sso0563, Sso0564 and Sso0566) were unchanged. We speculate that up-regulation of proteins involved in glycolysis was activated for energy requirements. Ultimately, these regulations supported the shorter lag phase of PBL2025 grown in tryptone media compared to glucose.

CONCLUSIONS

The current study investigates collectively responses at the proteome and metabolome levels of *S. solfatricus* strains P2 and PBL2025. The results allowed an improved understanding of

the metabolic alterations and varying levels of feedback-inhibition mechanisms that enabled the survival of the PBL2025 strain in the absence of 46 genes. As we seek to identify the ability of PBL2025 to mediate the most basic changes in carbon source, our studies have revealed distinct metabolic response and variations relating to carbohydrate and amino acid compounds. Differential regulation detected at nutrient transporter levels successfully showed unique ABC transporters that may have increased utilization by P2 and PBL2025, respectively. This clearly demonstrates the metabolic resilience at nutrient uptake level under stimuli introduced through changes in growth medium, while enabling future investigations to pinpoint specific/unique transporters for further characterization. Supported data from enrichment analysis also revealed increased regulation in post translational modifications (unpublished data), a correlation that supports earlier interest in phosphorylation modulation in P2 strains (10). These modulations in nutrient uptake can be correlated to changes we observed on growth and lag phases recorded during sampling. Other notable changes were also identified in carbon fixation metabolism and amino acid biosynthesis, as well as unique oligo/dipeptide superfamily transporters.

This study is the first, to our knowledge, that examine the collective and differing responses of global systems biology level changes differently under carbon source stimuli for *S. solfataricus* P2 and PBL2025. Our findings enable an important overview step to further understand extent of the environmental modulations and metabolic mechanism in the different *S. solfataricus* strains. It is particularly functionally useful due to the known genotypic differences between these two archaea.

SUPPORTING INFORMATION FILES

Supporting Tables

Table S1. Labelling of the 1st (A) and 2nd sets of iTRAQ experiments.

Table S2. Protein list for enrichment test.

Table S3. arCOG classification of regulated proteins.

Table S4. Comparison of transporter proteins detected in this study with literature.

Table S5. Metabolites identified with C number and their changed abundances.

Table S6. Proteomic data used for Figure 4 in relationship with literature.

Supporting Figures

Figure S1. The design of the 1st and 2nd set of iTRAQ experiments.

Figure S2. Classification of regulated proteins based on arCOG gene functions. PBL2025 *vs* P2 both grown on glucose, P2 grown on tryptone *vs* glucose, and PBL2025 grown on tryptone *vs* glucose.

Figure S3. Classification of regulated proteins based on arCOG gene functions. PBL2025 *vs* P2 both grown on glucose, P2 grown on tryptone *vs* glucose, and PBL2025 grown on tryptone *vs* glucose

Figure S4. Cloud plot from online XCMS statistical analysis of GC-MS data for different comparisons: PBL2025 *vs* P2 both grown on glucose, P2 grown on tryptone *vs* glucose, and PBL2025 grown on tryptone vs glucose.

ACKNOWLEDGEMENTS

WQ acknowledges UK-China scholarships for Excellence Programme and China Scholarship Council (CSC). PCW and TKP acknowledge the EPSRC (EP/E036252/1 and EP/1031812/1) and the BBSRC (BB/M018172/1) for financial support. We thank Professor Paul Blum at The University of Nebraska-Lincoln for kindly providing *S. solfataricus* PBL2025.

REFERENCES

1. Brock, T. D.; Brock, K. M.; Belly, R. T.; Weiss, R. L., Sulfolobus: a new genus of sulfur-oxidizing Bacteria living at low pH and high temperature. *Arch Mikrobiol* **1972,** 84, (1), 54-68.
2. Grogan, D., Phenotypic characterization of the archaebacterial genus Sulfolobus: comparison of five wild-type strains. *J Bacteriol* **1989,** 171, 6710-6719.
3. Zillig, W.; Stetter, K. O.; Wunderl, S.; Schulz, W.; Priess, H.; Scholz, I., The Sulfolobus-"Caldariella" group: Taxonomy on the basis of the structure of DNA-dependent RNA polymerases *Arch. Microbiol* **1980,** 125, (3), 259-269.
4. Rolfsmeier, M.; Blum, P., Purification and characterization of a maltase from the extremely thermophilic crenarchaeote Sulfolobus solfataricus. *J Bacteriol* **1995,** 177, (2), 482-485.
5. She, Q.; Singh, R. K.; Confalonieri F; Zivanovic Y; Allard G; Awayez MJ; Chan-Weiher CC; Clausen IG; Curtis BA; De Moors A; Erauso G; Fletcher C; Gordon PM; Heikamp-de Jong I; Jeffries AC; Kozera CJ; Medina N; Peng X; Thi-Ngoc HP; Redder P; Schenk ME; Theriault C; Tolstrup N; Charlebois RL; Doolittle WF; Duguet M; Gaasterland T; Garrett RA; Ragan MA; Sensen CW; Van der Oost J, The complete genome of the crenarchaeon Sulfolobus solfataricus P2. *Proc Natl Acad Sci U S A.* **2001,** 98, (14), 7835-7840.
6. Berkner, S.; Lipps, G., Genetic tools for Sulfolobus spp.: vectors and first applications. *Archives of microbiology* **2008,** 190, (3), 217-230.
7. Schelert, J.; Dixit, V.; Hoang, V.; Simbahan, J.; Drozda, M.; Blum, P., Occurrence and characterization of mercury resistance in the hyperthermophilic archaeon Sulfolobus solfataricus by use of gene disruption. *J Bacteriol* **2004,** 186, (2), 427-437.
8. Koerdt, A.; Jachlewski, S.; Ghosh, A.; Wingender, J.; Siebers, B.; Albers, S.-V., Complementation of Sulfolobus solfataricus PBL2025 with an α-mannosidase: effects on surface attachment and biofilm formation. *Extremophiles* **2012,** 16, (1), 115-125.
9. Snijders, A. P.; Walther, J.; Peter, S.; Kinnman, I.; De Vos, M. G.; Van de Werken, H. J.; Brouns, S. J.; Van der Oost, J.; Wright, P. C., Reconstruction of central carbon metabolism in Sulfolobus solfataricus using a two‐dimensional gel electrophoresis map, stable isotope labelling and DNA microarray analysis. *Proteomics* **2006,** 6, (5), 1518-1529.
10. Esser, D.; Pham, T.; Reimann, J.; Albers, S.; Siebers, B.; Wright, P., Change of carbon source causes dramatic effects in the phospho-proteome of the Archaeon Sulfolobus solfataricus. *J Proteome Res* **2012,** 11, (10), 4823-4833.
11. Zolghadr, B.; Klingl, A.; Koerdt, A.; Driessen, A. J.; Rachel, R.; Albers, S.-V., Appendage-mediated surface adherence of Sulfolobus solfataricus. *J Bacteriol* **2010,** 192, (1), 104-110.
12. Zaparty, M.; Esser, D.; Gertig, S.; Haferkamp, P.; Kouril, T.; Manica, A.; Pham, T. K.; Reimann, J.; Schreiber, K.; Sierocinski, P., "Hot standards" for the thermoacidophilic archaeon Sulfolobus solfataricus. *Extremophiles* **2010,** 14, (1), 119-142.
13. Ow, S. Y.; Salim, M.; Noirel, J.; Evans, C.; Rehman, I.; Wright, P. C., iTRAQ underestimation in simple and complex mixtures:"the good, the bad and the ugly". *J Proteome Res* **2009,** 8, (11), 5347-5355.
14. Elias, J. E.; Gygi, S. P., Target-decoy search strategy for increased confidence in large-scale protein identifications by mass spectrometry. *Nature methods* **2007,** 4, (3), 207-214.
15. Gusev, Y., Computational methods for analysis of cellular functions and pathways collectively targeted by differentially expressed microRNA. *Methods* **2008,** 44, (1), 61-72.
16. Pham, K. T.; Wright, P. C., The Proteomic Response of Saccharomyces cerevisiae in Very High Glucose Conditions with Amino Acid Supplementation. *J. Proteome Res.* **2008,** 7, (11), 4766-4774.
17. Meyer, M. R.; Peters, F. T.; Maurer, H. H., Automated mass spectral deconvolution and identification system for GC-MS screening for drugs, poisons, and metabolites in urine. *Clinical chemistry* **2010,** 56, (4), 575-584.
18. Bouatra, S.; Aziat, F.; Mandal, R.; Guo, A. C.; Wilson, M. R.; Knox, C.; Bjorndahl, T. C.; Krishnamurthy, R.; Saleem, F.; Liu, P., The human urine metabolome. *PloS one* **2013,** 8, (9), e73076.

19. Ogata, H.; Goto, S.; Sato, K.; Fujibuchi, W.; Bono, H.; Kanehisa, M., KEGG: Kyoto encyclopedia of genes and genomes. *Nucleic acids research* **1999,** 27, (1), 29-34.
20. Elferink, M. G. L.; Albers, S. V.; Konings, W. N.; Driessen, A. J. M., Sugar transport in Sulfolobus solfataricus is mediated by two families of binding protein - dependent ABC transporters. *Molecular microbiology* **2001,** 39, (6), 1494-1503.
21. Albers, S.-V.; Elferink, M. G.; Charlebois, R. L.; Sensen, C. W.; Driessen, A. J.; Konings, W. N., Glucose transport in the extremely thermoacidophilic Sulfolobus solfataricus involves a high-affinity membrane-integrated binding protein. *Journal of bacteriology* **1999,** 181, (14), 4285-4291.
22. Lalithambika, S.; Peterson, L.; Dana, K.; Blum, P., Carbohydrate hydrolysis and transport in the extreme thermoacidophile Sulfolobus solfataricus. *Appl. Environ. Microbiol* **2012,** 78, (22), 7931-7938.
23. Gogliettino M; Balestrieri M; Pocsfalvi G; Fiume I; Natale L; Rossi M; G, P., A highly selective oligopeptide binding protein from the archaeon Sulfolobus solfataricus. *J Bacteriol* **2010,** 192, (12), 3123-3131.
24. Konings, W. N.; Albers, S.-V.; Koning, S.; Driessen, A. J., The cell membrane plays a crucial role in survival of bacteria and archaea in extreme environments. *Antonie Van Leeuwenhoek* **2002,** 81, (1-4), 61-72.
25. White, D., The Physiology and Biochemistry of Prokaryotes. The 2nd edition. In New York: Oxford University Press: 2000. Chapter 8-9, 214-238.
26. Owen, O. E.; Kalhan, S. C.; Hanson, R. W., The key role of anaplerosis and cataplerosis for citric acid cycle function. *Journal of Biological Chemistry* **2002,** 277, (34), 30409-30412.
27. Ahmed, H.; Ettema, T. J.; Tjaden, B.; Geerling, A. C.; van der Oost, J.; Siebers, B., The semi-phosphorylative Entner–Doudoroff pathway in hyperthermophilic archaea: a re-evaluation. *Biochemical Journal* **2005,** 390, (Pt 2), 529.
28. Pettersson, H.-E., Growth of a mixed species lactic starter in a continuous "pH-Stat" fermentor. *Applied microbiology* **1975,** 29, (4), 437-443.
29. Moll, R.; Schäfer, G., Chemiosmotic H+ cycling across the plasma membrane of the thermoacidophilic archaebacterium Sulfolobus acidocaldarius. *FEBS letters* **1988,** 232, (2), 359-363.
30. Pham, T. K.; Roy, S.; Noirel, J.; Douglas, I.; Wright, P. C.; Stafford, G. P., A quantitative proteomic analysis of biofilm adaptation by the periodontal pathogen Tannerella forsythia. *Proteomics* **2010,** 10, (17), 3130-3141.
31. Bessarabova, M.; Ishkin, A.; JeBailey, L.; Nikolskaya, T.; Nikolsky, Y., Knowledge-based analysis of proteomics data. *BMC bioinformatics* **2012,** 13, (Suppl 16), S13.
32. Pham, T. K.; Sierocinski, P.; van der Oost, J.; Wright, P. C., Quantitative proteomic analysis of Sulfolobus solfataricus membrane proteins. *Journal of proteome research* **2010,** 9, (2), 1165-1172.
33. Chong, P. K.; Burja, A. M.; Radianingtyas, H.; Fazeli, A.; Wright, P. C., Proteome analysis of Sulfolobus solfataricus P2 propanol metabolism. *J Proteome Res* **2007,** 6, (4), 1430-1439.
34. Chong, P. K.; Burja, A. M.; Radianingtyas, H.; Fazeli, A.; Wright, P. C., Translational and transcriptional analysis of Sulfolobus solfataricus P2 to provide insights into alcohol and ketone utilisation. *Proteomics* **2007,** 7, (3), 424-435.
35. Chong, P. K.; Burja, A. M.; Radianingtyas, H.; Fazeli, A.; Wright, P. C., Proteome and transcriptional analysis of ethanol-grown Sulfolobus solfataricus P2 reveals ADH2, a potential alcohol dehydrogenase. *Journal of proteome research* **2007,** 6, (10), 3985-3994.
36. Albers, S. V.; Koning, S. M.; Konings, W. N.; Driessen, A. J. M., Insights into ABC transport in archaea. *Journal of bioenergetics and biomembranes* **2004,** 36, (1), 5-15.
37. Kort, J. C.; Esser, D.; Pham, T. K.; Noirel, J.; Wright, P. C.; Siebers, B., A cool tool for hot and sour Archaea: Proteomics of Sulfolobus solfataricus. *Proteomics* **2013,** 13, (18-19), 2831-2850.
38. Kouril, T.; Wieloch, P.; Reimann, J.; Wagner, M.; Zaparty, M.; Albers, S. V.; Schomburg, D.; Ruoff, P.; Siebers, B., Unraveling the function of the two Entner–Doudoroff branches in the thermoacidophilic Crenarchaeon Sulfolobus solfataricus P2. *FEBS Journal* **2013,** 280, (4), 1126-1138.
39. Fukushima, A.; Kusano, M.; Redestig, H.; Arita, M.; Saito, K., Metabolomic correlation-network modules in Arabidopsis based on a graph-clustering approach. *BMC systems biology* **2011,** 5, (1), 1.

40. Bar-Even, A.; Noor, E.; Milo, R., A survey of carbon fixation pathways through a quantitative lens. *Journal of experimental botany* **2012,** 63, (6), 2325-2342.
41. Haferkamp, P.; Kutschki, S.; Treichel, J.; Hemeda, H.; Sewczyk, K.; Hoffmann, D.; Zaparty, M.; Siebers, B., An additional glucose dehydrogenase from Sulfolobus solfataricus: fine-tuning of sugar degradation? *Biochemical Society Transactions* **2011,** 39, (1), 77.
42. Brosnan, J. T., Interorgan amino acid transport and its regulation. *The Journal of nutrition* **2003,** 133, (6), 2068S-2072S.
43. Umbarger, H. E., Amino acid biosynthesis and its regulation. *Annual review of biochemistry* **1978,** 47, (1), 533-606.
44. Adelberg, E. A.; Umbarger, H. E., Isoleucine and valine metabolism in Escherichia coli. *Journal of Biological Chemistry* **1953,** 205, (1), 475-482.
45. Umbarger, H. E.; Brown, B., Isoleucine and valine metabolism in Escherichia coli. *Journal of Biological Chemistry* **1958,** 233, (2), 415.
46. Knöchel, T.; Ivens, A.; Hester, G.; Gonzalez, A.; Bauerle, R.; Wilmanns, M.; Kirschner, K.; Jansonius, J. N., The crystal structure of anthranilate synthase from Sulfolobus solfataricus: functional implications. *Proceedings of the National Academy of Sciences* **1999,** 96, (17), 9479-9484.
47. Brosnan, J. T.; Brosnan, M. E., Branched-chain amino acids: enzyme and substrate regulation. *The Journal of nutrition* **2006,** 136, (1), 207S-211S.
48. Park, C. B.; Lee, S. B., Effects of exogenous compatible solutes on growth of the hyperthermophilic archaeon *Sulfolobus solfataricus*. *Journal of bioscience and bioengineering* **2000,** 89, (4), 318-322.
49. Feehily, C.; Karatzas, K.-A. G., Role of glutamate metabolism in bacterial responses towards acid and other stresses. *Journal of applied microbiology* **2013,** 114, (1), 11-24.
50. Diez‐Gonzalez, F.; Karaibrahimoglu, Y., Comparison of the glutamate‐, arginine‐and lysine‐dependent acid resistance systems in Escherichia coli O157: H7. *Journal of applied microbiology* **2004,** 96, (6), 1237-1244.
51. Bearson, B. L.; Lee, I. S.; Casey, T. A., Escherichia coli O157: H7 glutamate-and arginine-dependent acid-resistance systems protect against oxidative stress during extreme acid challenge. *Microbiology* **2009,** 155, (3), 805-812.
52. Álvarez-Ordóñez, A.; Fernández, A.; Bernardo, A.; López, M., Arginine and lysine decarboxylases and the Acid Tolerance Response of *Salmonella Typhimurium*. *International journal of food microbiology* **2010,** 136, (3), 278-282.
53. Consalv, V.; Chiaraluce, R.; Politi, L.; Gambacorta, A.; Rosa, M.; Scandurra, R., Glutamate dehydrogenase from the thermoacidophilic archaebacterium Sulfolobus solfataricus. *European journal of biochemistry* **1991,** 196, (2), 459-467.
54. Sanangelantoni, A. M.; Barbarini, D.; Di Pasquale, G.; Cammarano, P.; Tiboni, O., Cloning and nucleotide sequence of an archaebacterial glutamine synthetase gene: phylogenetic implications. *Molecular and General Genetics MGG* **1990,** 221, (2), 187-194.
55. Yin, Z.; Purschke, W. G.; Schäfer, G.; Schmidt, C. L., The glutamine synthetase from the hyperthermoacidophilic crenarcheon Sulfolobus acidocaldarius: isolation, characterization and sequencing of the gene. *Biological Chemistry* **1998,** 379, (11), 1349-1354.
56. Alberts, B.; Johnson, A.; Lewis, J.; Raff, M.; Roberts, K.; Walter, P., Chloroplasts and Photosynthesis. The 4th edition. New York: Garland Science : **2002**, Chapter 14, 813-878.
57. Berg, I. A.; Kockelkorn, D.; Buckel, W.; Fuchs, G., A 3-hydroxypropionate/4-hydroxybutyrate autotrophic carbon dioxide assimilation pathway in Archaea. *Science* **2007,** 318, (5857), 1782-1786.
58. Rich, P. R., The molecular machinery of Keilin's respiratory chain. *Biochemical Society Transactions* **2003,** 31, 1095-1105.

TABLE AND FIGURE LEGENDS

Table Legends

Table 1. Numbers of identified and quantified proteins from iTRAQ experiments.

Table 2. (A) Comparisons of the number of compounds detected from different *S. solfataricus* strains grown on different carbon sources. (B) Representative compounds identified from different comparisons.

Table 3. Summary of pathway enrichment analysis (hypergeometric model) result.

Figure Legends

Figure 1. Growth profiles of *S. solfataricus* P2 (●) and PBL2025 (○) in 0.4% (w/v) glucose (A) and 0.2% (w/v) tryptone (B) media, plotted as natural log of cell density as a function of time. (C) Specific growth rates of *S. solfataricus* P2 and PBL2025 strains grown on 0.4% (w/v) glucose and 0.2% (w/v) tryptone. Glucose consumption profiles of *S. solfataricus* P2 (●) and PBL2025 (○) grown on 0.4% (w/v) glucose (D). Data were generated from biological triplicate cultures.

Figure 2. The pH change of medium against the cell growth for *S. solfataricus* P2 (○, ●) and PBL2025 (◊, ♦) grown on different carbon sources. (Open and filled symbols for 0.2% tryptone and 0.4% glucose respectively).

Figure 3. Venn diagram of identified compounds from: Both strains grown on glucose (A); *S. solfataricus* P2 (B) and PBL2025 (C) grown on different carbon sources.

Figure 4. Regulated metabolism pathways for comparison 1: PBL2025 *vs* P2 both grown on glucose (purple); comparison 2: tryptone *vs* glucose of P2 (green); comparison 3: tryptone *vs* glucose of PBL2025 (red). CCM including glycolysis, TCA and pyruvate metabolism (A). Symbols ↑ and ↓ indicate up-regulated and down-regulated proteins respectively. Reconstruction of carbohydrate metabolism and biosynthesis of amino acids (B). Rectangles with broken lines represent metabolites. Rectangles with solid lines represent proteins. Fold change >1, <1 and =1 indicate up-regulated, down-regulated and un-changed, respectively. G1P: glucose 1-phosphate; G6P: glucose 6-phosphate; F6P: fructose 6-phosphate; F1,6P: fructose 1,6-bisphosphate; DHAP: dihydroxyacetone 3-phosphate; KD(P)G: 2-keto-3-deoxy-(6-phospho)gluconate; GAP: glyceraldehyde 3-phosphate; PGP: 1,3-bisphosphoglycerate; 3-

PG: 3-phosphoglycerate; 2-PG: 2-phosphoglycerate; GA: glyceraldehyde; PEP: posphoenolpyruvate; PPP: pentose phosphate pathway; OAA: oxaloacetic acid; OGA: 2-oxoglutarate; IPMI: 3-isopropylmalate dehydratase, small subunit (isopropylmalate isomerase) (alpha IPM isomerase); leuA-2: 2-isopropylmalate synthase.

TABLES

Table 1. Numbers of identified and quantified proteins from iTRAQ experiments.

Total predicted proteins[a)]	2994					
iTRAQ experiment	1st experiment				2nd experiment	
Proteins identified with ≥ 2 MS/MS spectra[b)]	583				609	
Protein regulation	Number of proteins and their distribution (%)					
	PBL2025 *vs* P2 both grown on glucose		P2 grown on tryptone *vs* glucose		PBL2025 grown on tryptone *vs* glucose	
Up	97	16.6%	78	13.4%	110	18.1%
Unchanged	425	72.9%	424	72.7%	401	65.8%
Down	61	10.5%	81	13.9%	98	16.1%

a) She, et al., 2001. B) ≥ 2 peptides and FDR < 0.01.

Table 2A Comparisons of the number of compounds detected from different *S. solfataricus* strains grown on different carbon sources.

Carbon source	Strains	Replicates				Merge data	Merge data from 2 strains
		3	4	5	6		
Glucose	P2	2	7	81	10	100	
	PBL2025	2	20	18	82	122	130
Tryptone	P2	5	11	20	91	127	
	PBL2025	2	29	67	0	98	128

Notes: Biological triplicates and technical duplicates were run for each experiment. The number 3-6 indicates that metabolites were detected from 3 (biological triplicates), or 4, or 5, or 6 GC-MS runs. Metabolites determined only from 1 or 2 biological samples are not considered.

Table 2B Representative compounds identified from different comparisons.

Category	Metabolites	Glucose	Tryptone	Tryptone/Glucose	
		2025/P2	2025/ P2	P2	PBL2025
Metabolic intermediates	Acetyl-L-alanine	1.79	0	0.99	~
	3-Iodo-L-tyrosine	2.21	0	3.01	0
	Methylglutamic acid	NF	1.25	~	~
	Pyroglutamic acid	6.64	4.87	5.93	4.35
	1-Methylguanine	4.63	1.88	2.31	0.93
Amino acids	Alanine	6.21	1.36	2.76	0.6
	Glutamic acid	3.84	2.37	4.67	2.88
	Glutamine	5.22	0	7.05	0
	Glycine	2.58	4.89	0.82	1.55
	Leucine	2.18	1.06	2.09	1.02
	Phenylalanine	1.37	0	2.01	0
	Proline	2.18	1.92	2.09	~
	Serine	2.46	0.3	13.74	1.68
	Threonine	6.89	0	2.42	0
	Tyrosine	2.23	1.31	2.99	1.76
	Tryptophan	0	0	2.46	NF
Other metabolites	Acetic acid	2.51	3.47	1.01	1.39
	Glyceraldehyde	0	NF	0	NF
	α-ketoglutaric acid	3.56	NF	0	0
	Lactic acid	5.89	3.6	2.61	1.6
	Urea	2.24	NF	0	0

Note: 0 indicates that metabolites only not detected in 'divisor' condition. ~ indicates that metabolite is not detected in 'dividended' condition. NF indicates not found. The 'area' was normalized using external standard Nor-valine and ratio was calculated.

Table 3 Summary of pathway enrichment analysis (hypergeometric model) result.

	Pathways	C1	C2	C3
Carbohydrate metabolism	Butanoate metabolism	+	None	None
	Glycolysis	None	_	+
	Pyruvate metabolism	None	_	None
Amino acids metabolism	Ala, asp and glu metabolism	_	+	_
	Arg and pro metabolism	_	_	None
	Val, leu and iso-leu biosynthesis	+	_	_
	Val, leu and iso-leu biodegradation	None	_	None
Energy metabolism	Carbon fixation pathways	+	None	None
	Oxidative phosphorylation	None	None	_
Nucleotide metabolism	Purine metabolism	None	_	None
	Pyrimidine metabolism	None	_	None

Note: C1: PBL2025 *vs* P2 both grown on glucose; C2: P2 grown on tryptone *vs* glucose; C3: PBL2025 grown on tryptone *vs* glucose. +: Up regulation. -: Down regulation. None: change was not significant in a given pathway. A pathway was considered if more than 5 quantified proteins were observed for that pathway.

FIGURES

Figure 1.

(A)

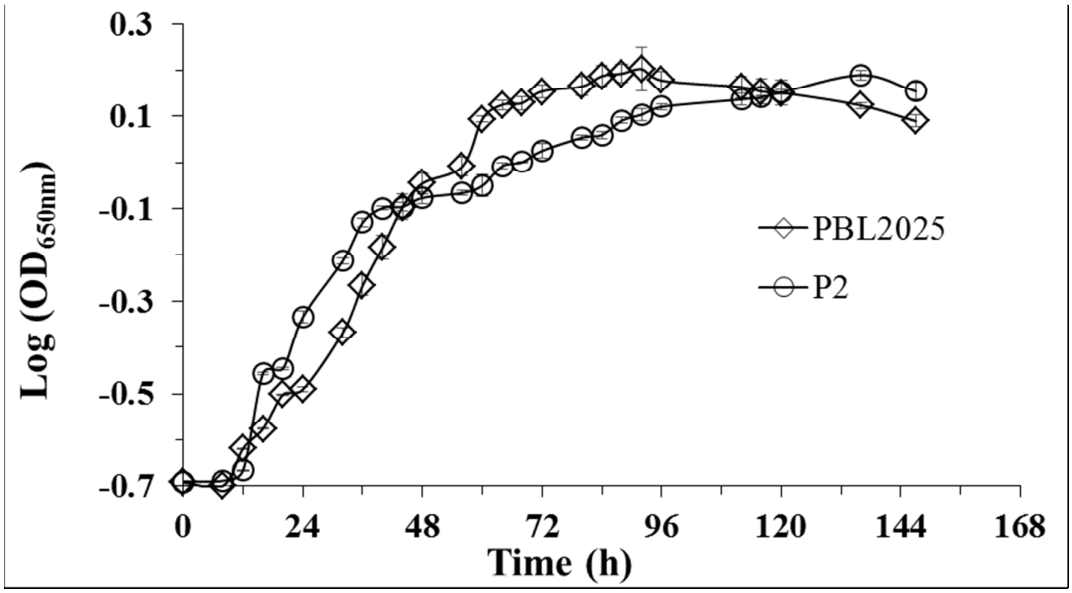

(B)

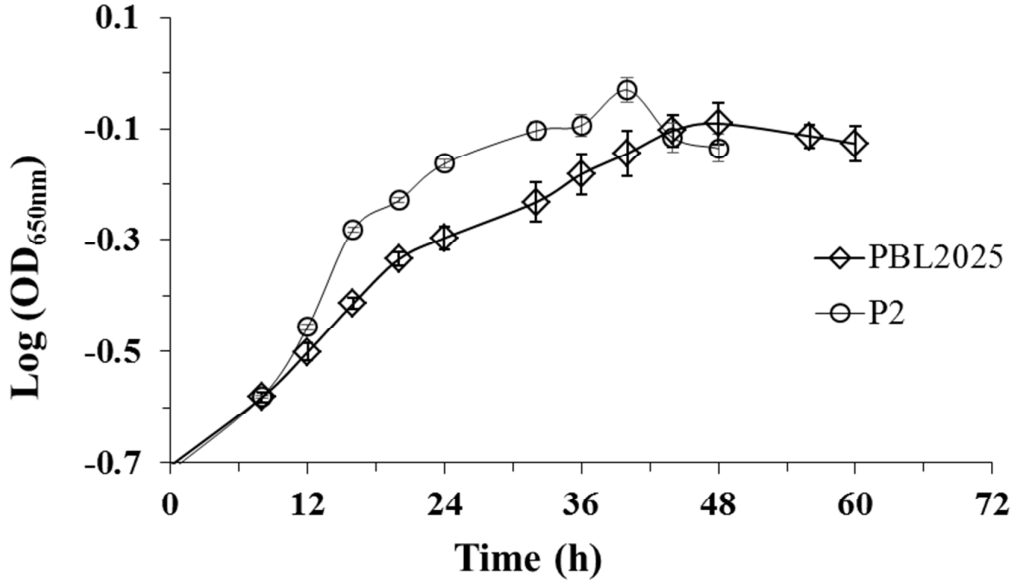

(C)

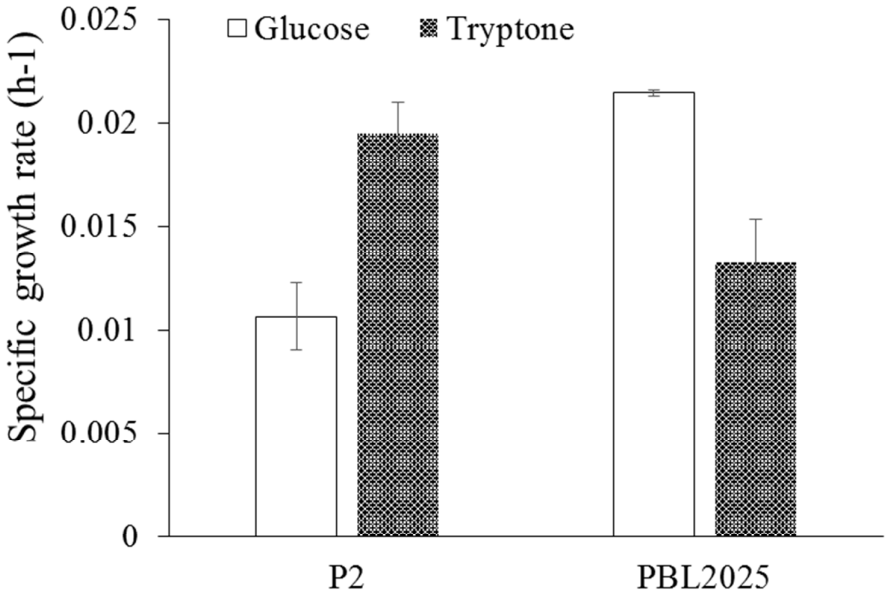
Glucose
Tryptone
Specific growth rate (h-1)
0.025
0.02
0.015
0.01
0.005
0
P2
PBL2025

(D)

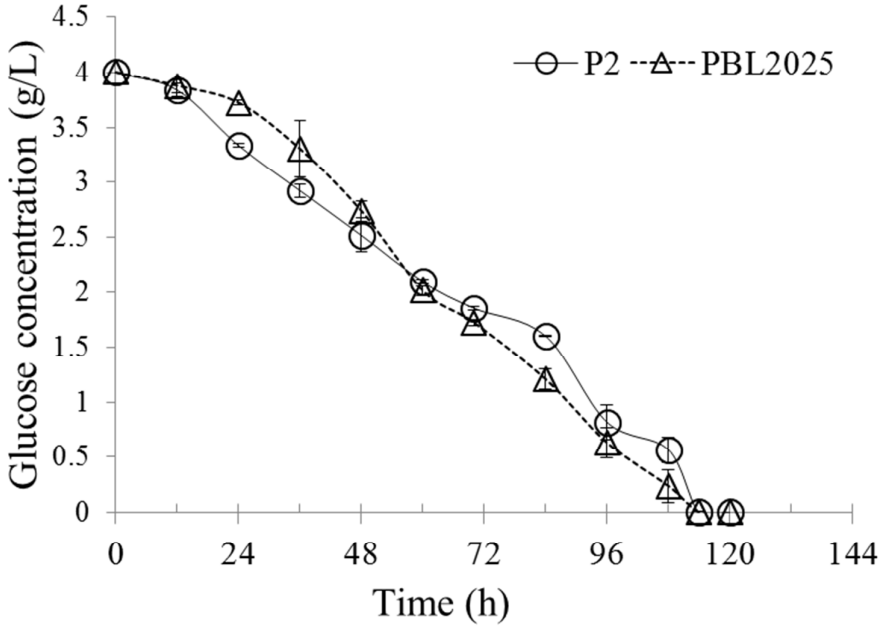
P2
PBL2025
Glucose concentration (g/L)
4.5
4
3.5
3
2.5
2
1.5
1
0.5
0
0
24
48
72
96
120
144
Time (h)

Figure 2.

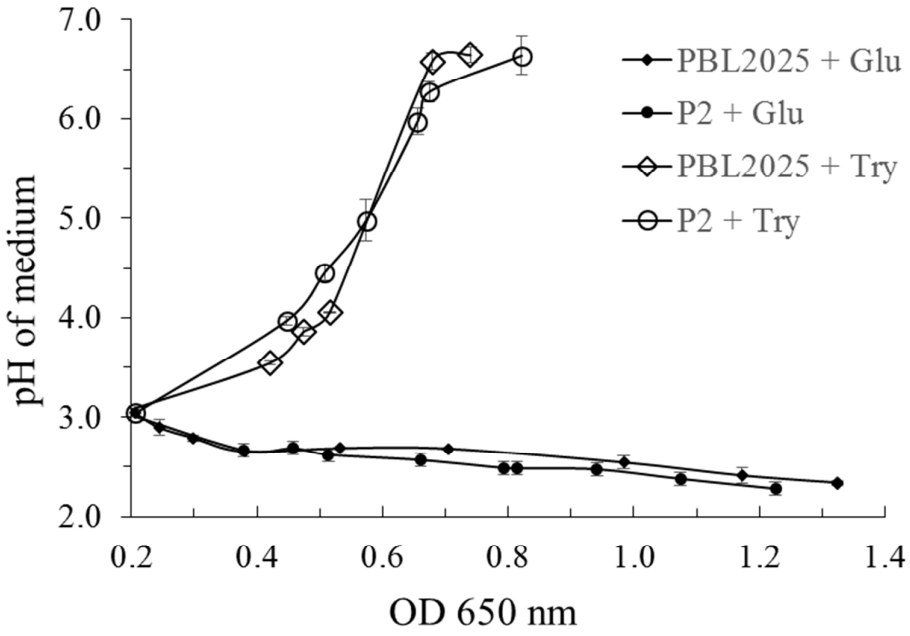

Figure 3

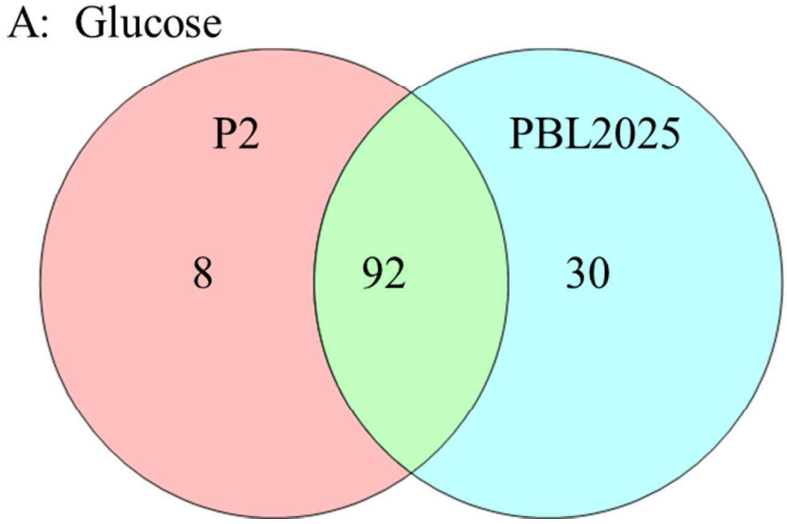

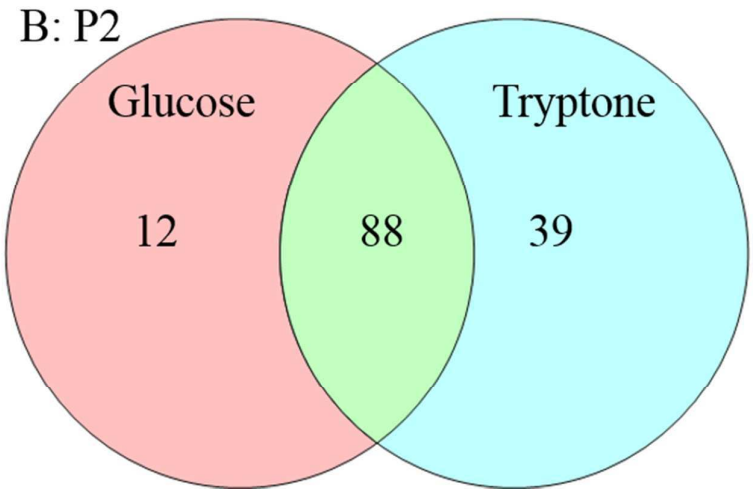
B: P2
Glucose
Tryptone
12
88
39

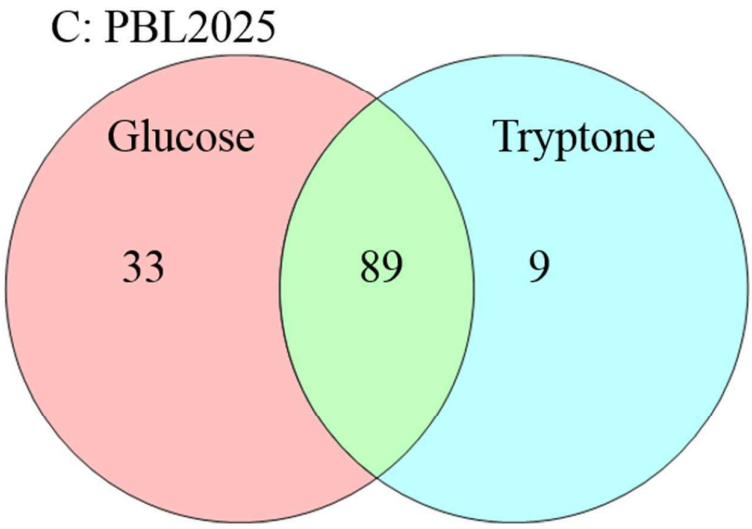
C: PBL2025
Glucose
Tryptone
33
89
9

Figure 4A

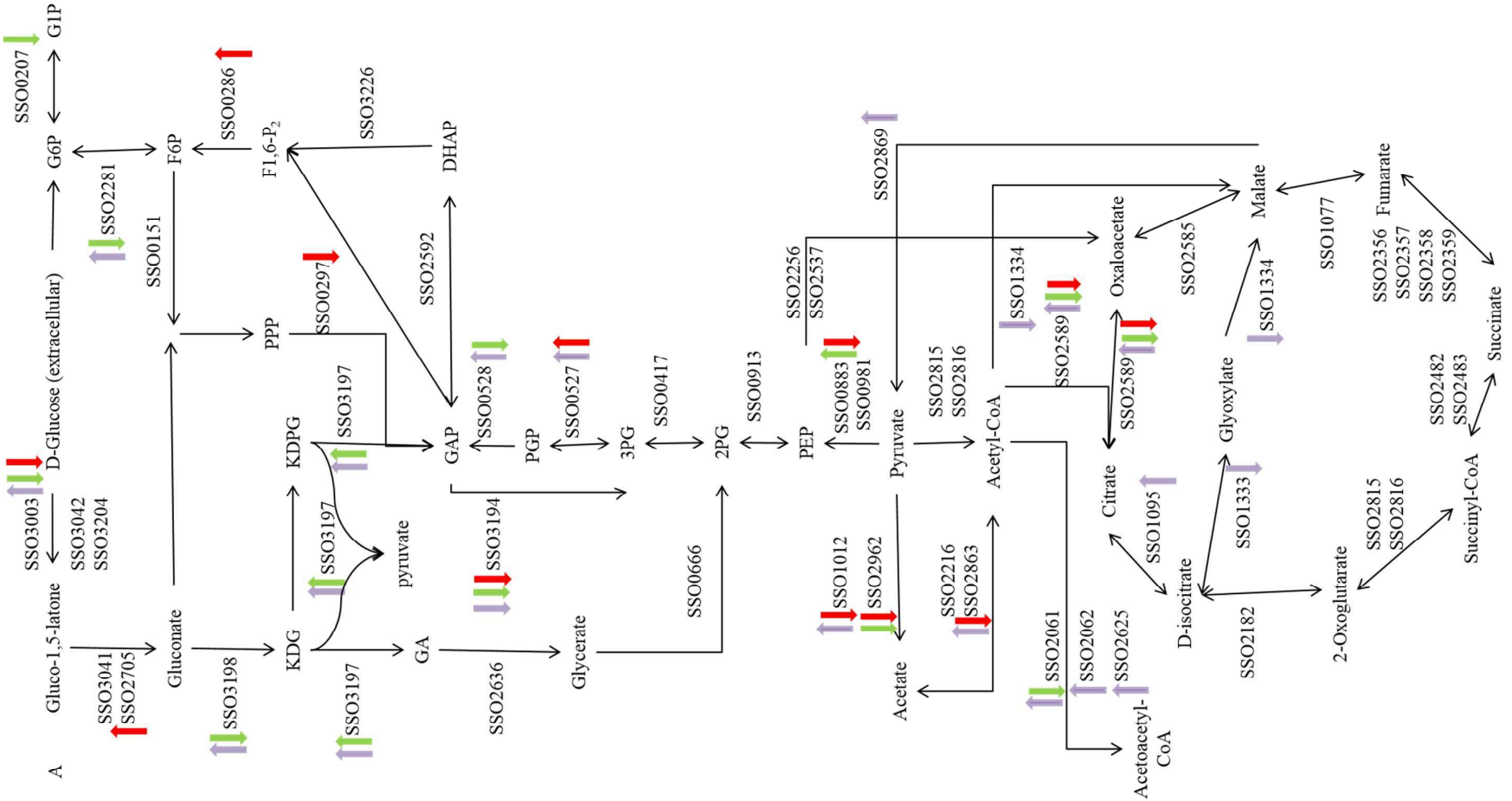
SSO0207
G1P
G6P
SSO2281
F6P
SSO0286
F1,6-P2
SSO3226
DHAP
SSO0151
SSO0297
SSO2592
PPP
KDPG
SSO3197
GAP
SSO0528
PGP
SSO0527
3PG
SSO0417
2PG
SSO0913
PEP
SSO0883
SSO0981
Pyruvate
SSO2815
SSO2816
Acetyl-CoA
SSO2256
SSO2537
SSO2869
SSO1334
SSO2589
Oxaloacetate
SSO2585
Malate
SSO1077
Fumarate
SSO2356
SSO2357
SSO2358
SSO2359
Succinate
SSO2482
SSO2483
Succinyl-CoA
SSO3003
D-Glucose (extracellular)
SSO3042
SSO3204
Gluco-1,5-latone
SSO3041
SSO2705
A
Gluconate
SSO3198
KDG
SSO3197
pyruvate
SSO3197
GA
SSO3194
SSO2636
Glycerate
SSO0666
SSO1012
SSO2962
Acetate
SSO2216
SSO2863
SSO2061
SSO2062
SSO2625
Acetoacetyl-CoA
Citrate
SSO1095
D-isocitrate
SSO1333
Glyoxylate
SSO1334
SSO2182
2-Oxoglutarate
SSO2815
SSO2816

Figure 4B

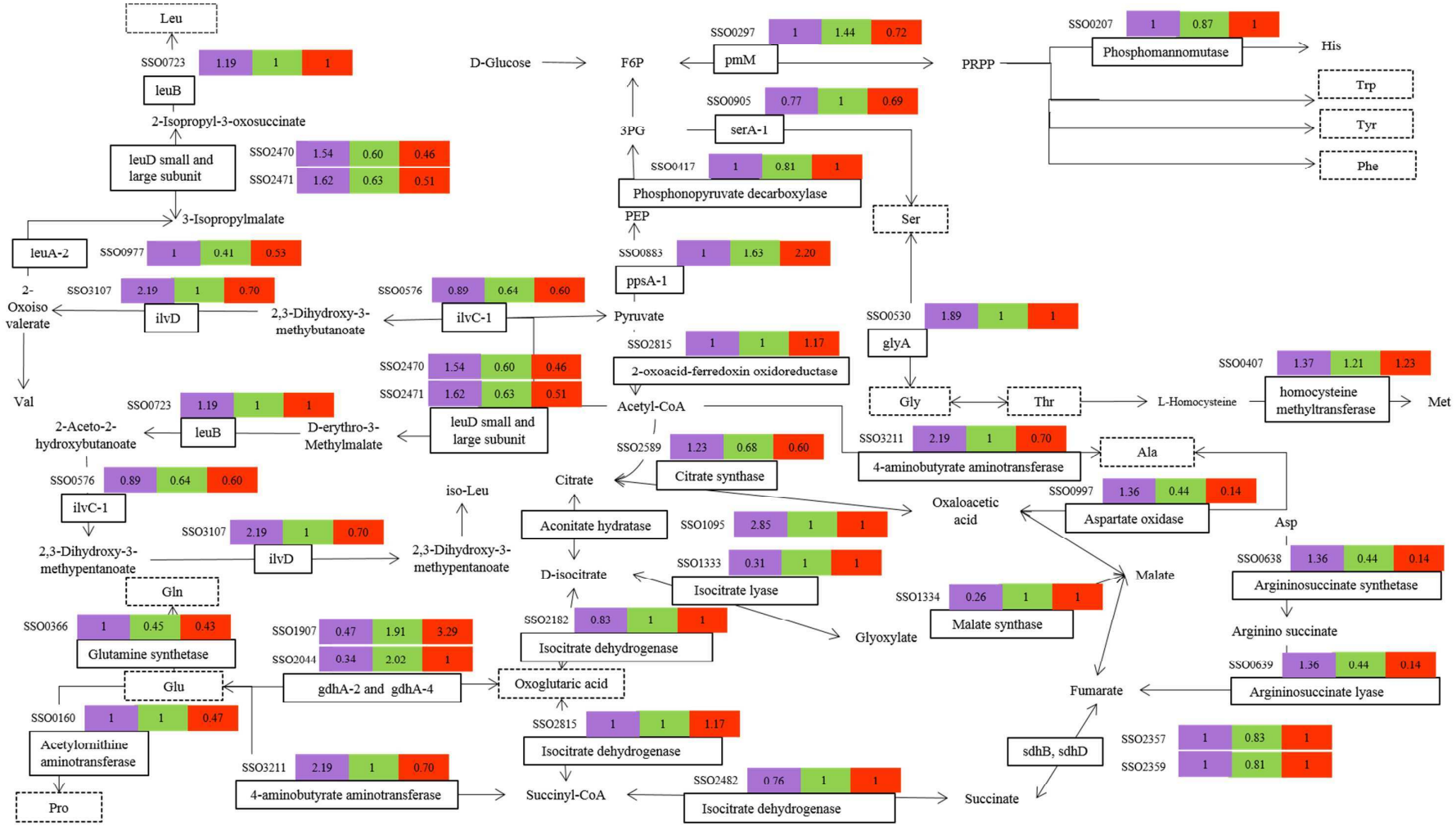
Leu
SSO0723 1.19 1 1
leuB
2-Isopropyl-3-oxosuccinate
leuD small and large subunit
SSO2470 1.54 0.60 0.46
SSO2471 1.62 0.63 0.51
3-Isopropylmalate
leuA-2
SSO0977 1 0.41 0.53
2-Oxoiso valerate
SSO3107 2.19 1 0.70
ilvD
2,3-Dihydroxy-3-methybutanoate
SSO0576 0.89 0.64 0.60
ilvC-1
Val
SSO0723 1.19 1 1
leuB
2-Aceto-2-hydroxybutanoate
D-erythro-3-Methylmalate
SSO2470 1.54 0.60 0.46
SSO2471 1.62 0.63 0.51
leuD small and large subunit
SSO0576 0.89 0.64 0.60
ilvC-1
2,3-Dihydroxy-3-methypentanoate
SSO3107 2.19 1 0.70
ilvD
2,3-Dihydroxy-3-methypentanoate
iso-Leu
Gln
SSO0366 1 0.45 0.43
Glutamine synthetase
Glu
SSO1907 0.47 1.91 3.29
SSO2044 0.34 2.02 1
gdhA-2 and gdhA-4
SSO0160 1 1 0.47
Acetylornithine aminotransferase
Pro
SSO3211 2.19 1 0.70
4-aminobutyrate aminotransferase
D-Glucose
F6P
SSO0297 1 1.44 0.72
pmM
PRPP
SSO0207 1 0.87 1
Phosphomannomutase
His
Trp
Tyr
Phe
SSO0905 0.77 1 0.69
3PG
serA-1
SSO0417 1 0.81 1
Phosphonopyruvate decarboxylase
PEP
Ser
SSO0883 1 1.63 2.20
ppsA-1
Pyruvate
SSO0530 1.89 1 1
glyA
SSO2815 1 1 1.17
2-oxoacid-ferredoxin oxidoreductase
Acetyl-CoA
Gly
Thr
L-Homocysteine
SSO0407 1.37 1.21 1.23
homocysteine methyltransferase
Met
SSO2589 1.23 0.68 0.60
Citrate synthase
Citrate
SSO3211 2.19 1 0.70
4-aminobutyrate aminotransferase
Ala
Oxaloacetic acid
SSO0997 1.36 0.44 0.14
Aspartate oxidase
Asp
Aconitate hydratase
SSO1095 2.85 1 1
D-isocitrate
SSO1333 0.31 1 1
Isocitrate lyase
Glyoxylate
SSO1334 0.26 1 1
Malate synthase
Malate
SSO0638 1.36 0.44 0.14
Argininosuccinate synthetase
Arginino succinate
SSO2182 0.83 1 1
Isocitrate dehydrogenase
Oxoglutaric acid
SSO0639 1.36 0.44 0.14
Argininosuccinate lyase
Fumarate
SSO2815 1 1 1.17
Isocitrate dehydrogenase
Succinyl-CoA
SSO2482 0.76 1 1
Isocitrate dehydrogenase
Succinate
sdhB, sdhD
SSO2357 1 0.83 1
SSO2359 1 0.81 1

For TOC Only

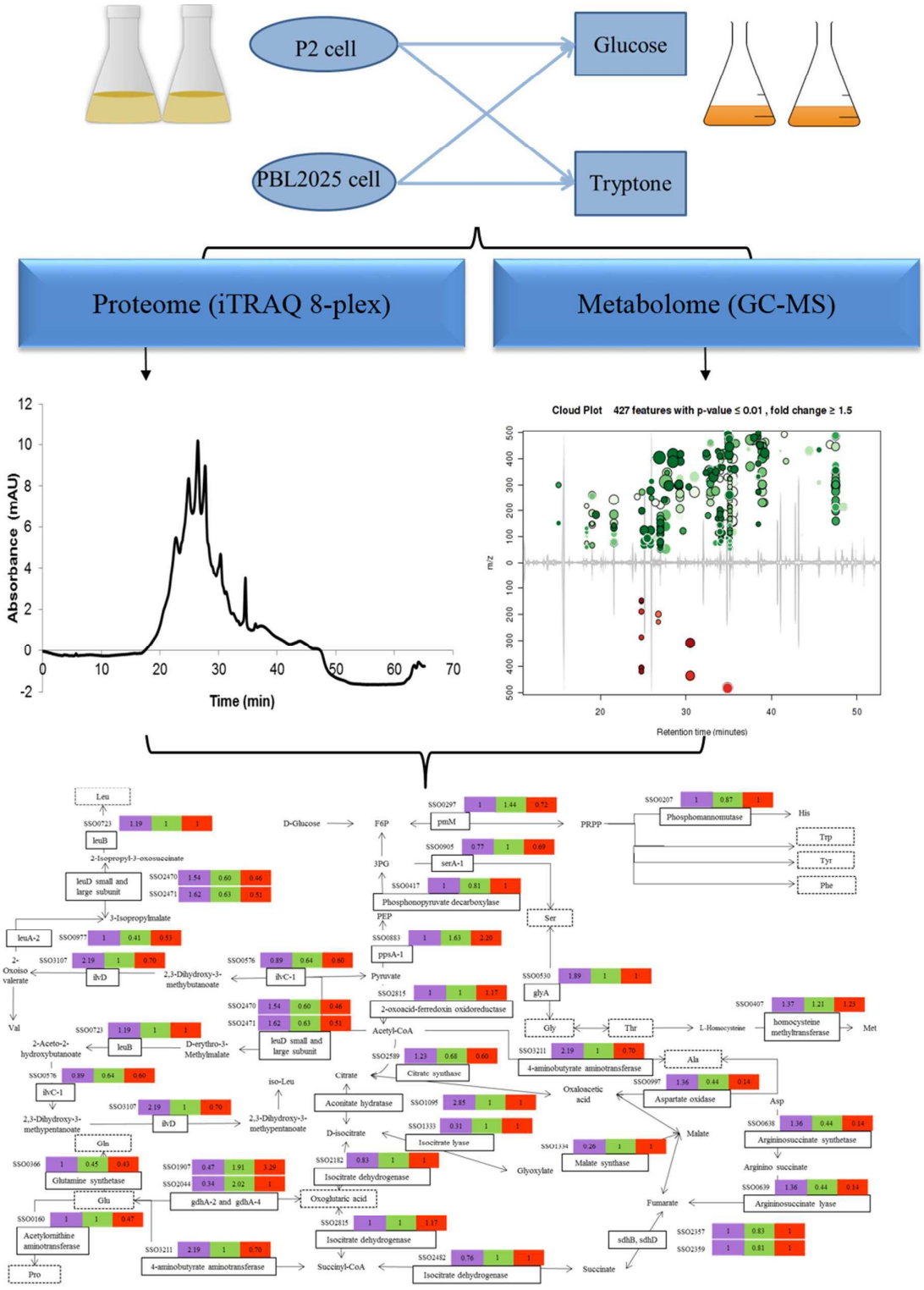
P2 cell
PBL2025 cell
Glucose
Tryptone
Proteome (iTRAQ 8-plex)
Metabolome (GC-MS)
Absorbance (mAU)
Time (min)
Cloud Plot 427 features with p-value ≤ 0.01 , fold change ≥ 1.5
m/z
Retention time (minutes)
Leu
leuB
2-Isopropyl-3-oxosuccinate
leuD small and large subunit
3-Isopropylmalate
leuA-2
2-Oxoisovalerate
ilvD
2,3-Dihydroxy-3-methylbutanoate
ilvC-1
Pyruvate
Val
2-Aceto-2-hydroxybutanoate
D-erythro-3-Methylmalate
iso-Leu
2,3-Dihydroxy-3-methylpentanoate
Gln
Glutamine synthetase
Glu
gdhA-2 and gdhA-4
Acetylornithine aminotransferase
Pro
4-aminobutyrate aminotransferase
D-Glucose
F6P
pmM
PRPP
Phosphomannomutase
His
Trp
Tyr
Phe
3PG
serA-1
Phosphonopyruvate decarboxylase
Ser
PEP
ppsA-1
2-oxoacid-ferredoxin oxidoreductase
Acetyl-CoA
Citrate synthase
Citrate
Aconitate hydratase
D-isocitrate
Isocitrate lyase
Glyoxylate
Malate synthase
Isocitrate dehydrogenase
Oxoglutaric acid
Succinyl-CoA
Succinate
glyA
Gly
Thr
L-Homocysteine
homocysteine methyltransferase
Met
4-aminobutyrate aminotransferase
Ala
Oxaloacetic acid
Aspartate oxidase
Asp
Malate
Argininosuccinate synthetase
Arginino succinate
Argininosuccinate lyase
Fumarate
sdhB, sdhD